Published November 19, 2012

Mutual antagonism between IP_3RII and miRNA-133a regulates calcium signals and cardiac hypertrophy

Faye M. Drawnel,[1] Dagmar Wachten,[1,2] Jeffery D. Molkentin,[3] Marjorie Maillet,[3] Jan Magnus Aronsen,[4,5] Fredrik Swift,[4] Ivar Sjaastad,[4] Ning Liu,[6] Daniele Catalucci,[7,8] Katsuhiko Mikoshiba,[9] Chihiro Hisatsune,[9] Hanneke Okkenhaug,[1] Simon R. Andrews,[1] Martin D. Bootman,[1] and H. Llewelyn Roderick[1,10]

[1]Babraham Institute, Babraham, Cambridge CB22 3AT, England, UK
[2]Department of Molecular Sensory Systems, Center of Advanced European Studies and Research, 53175 Bonn, Germany
[3]Department of Pediatrics, University of Cincinnati, Cincinnati Children's Hospital Medical Center, Cincinnati, OH 45229
[4]Institute for Experimental Medical Research, Faculty of Medicine, Oslo University Hospital, 0407 Oslo, Norway
[5]Bjørknes College, 0456 Oslo, Norway
[6]Department of Molecular Biology, UT Southwestern Medical Center, Dallas, TX 75390
[7]Humanitas Clinical and Research Center, 20089 Rozzano, Milan, Italy
[8]Institute of Genetic and Biomedical Research, Milan Section, National Research Council, 20138 Milan, Italy
[9]Laboratory for Developmental Neurobiology, RIKEN Brain Science Institute, Wako, Saitama 531-0198, Japan
[10]Department of Pharmacology, University of Cambridge, Cambridge CB2 1PD, England, UK

Inositol 1,4,5′-triphosphate receptor II (IP_3RII) calcium channel expression is increased in both hypertrophic failing human myocardium and experimentally induced models of the disease. The ectopic calcium released from these receptors induces pro-hypertrophic gene expression and may promote arrhythmias. Here, we show that IP_3RII expression was constitutively restrained by the muscle-specific miRNA, miR-133a. During the hypertrophic response to pressure overload or neurohormonal stimuli, miR-133a down-regulation permitted IP_3RII levels to increase, instigating pro-hypertrophic calcium signaling and concomitant pathological remodeling. Using a combination of in vivo and in vitro approaches, we demonstrated that IP_3-induced calcium release (IICR) initiated the hypertrophy-associated decrease in miR-133a. In this manner, hypertrophic stimuli that engage IICR set a feed-forward mechanism in motion whereby IICR decreased miR-133a expression, further augmenting IP_3RII levels and therefore pro-hypertrophic calcium release. Consequently, IICR can be considered as both an initiating event and a driving force for pathological remodeling.

Introduction

Left ventricular hypertrophy is a maladaptive response to cardiac insults such as hypertension, damage, or aging (Dorn, 2007), and predisposes to heart failure and sudden death (Haider et al., 1998). Initially, the heart is enlarged through hypertrophy of individual cardiomyocytes and extensive fibrosis within the ventricular wall. As the condition evolves, myocyte death is common and promotes the progression to heart failure. Studies in both animals and humans have indicated that remediation of the hypertrophic phenotype at the early stages of the disease improves outcome without compromising cardiac function (Hill et al., 2000; Kjeldsen et al., 2002). Hence, gaining a greater understanding of the mechanisms responsible for left ventricular hypertrophy may suggest novel therapeutic strategies.

Structural and molecular remodeling instigates pathological growth of the heart. Many of these maladaptive changes develop as a result of altered cardiomyocyte transcriptional

F.M. Drawnel and D. Wachten contributed equally to this paper.

Correspondence to H. Llewelyn Roderick: llewelyn.roderick@babraham.ac.uk

Abbreviations used in this paper: 3′UTR, 3′ untranslated region; 5P, 5′-phosphatase; AB, aortic banded; ANF, atrial natriuretic factor; ARVM, adult rat ventricular myocyte; CaMKII, calmodulin-dependent kinase II; CLNX, calnexin; Cn, calcineurin; CSQ, calsequestrin; dKO, double knockout; DN, dominant negative; ET-1, endothelin-1; HDAC, histone deacetylase; HEK, human endothelial kidney; HOP, homeodomain-only protein; IICR, IP_3-induced calcium release; IP_3, inositol-(1,4,5) triphosphate; IP_3RII, IP_3 receptor II; KO, knockout; miRNA, micro RNA; NFAT, nuclear factor of activated T cells; NRVM, neonatal rat ventricular myocyte; qPCR, quantitative real-time polymerase chain reaction; SHR, spontaneously hypertensive rat; SRF, serum response factor; TAC, thoracic aortic constriction; TP, target protector; TsA, trichostatin A; tTA, tetracycline transactivator; WKY, Wistar Kyoto; WT, wild type.

Supplemental Material can be found at:
http://jcb.rupress.org/content/suppl/2012/11/15/jcb.201111095.DC1.html

The Rockefeller University Press $30.00
J. Cell Biol. Vol. 199 No. 5 783–798
www.jcb.org/cgi/doi/10.1083/jcb.201111095

Published November 19, 2012

profiles, induced through the coordinated action of a network of transcription factors activated by neurohormonal stimuli and/or stretch (Wu et al., 2006; Higazi et al., 2009). This produces genome-wide changes in gene expression and permits expression of the proteins responsible for pathological myocardial growth. Signaling pathways regulated by changes in intracellular calcium are central to the transduction of pro-hypertrophic stimuli, governing the activation of transcriptional regulatory mechanisms including calcineurin-nuclear factor of activated T cells (Cn-NFAT; Higazi et al., 2009; Nakayama et al., 2010; Rinne and Blatter, 2010) and CaM-dependent kinase II–histone deacetylase 4–myocyte enhancer factor 2 (CaMKII–HDAC4–MEF2; Wu et al., 2006). During hypertrophy and heart failure, activity of these regulators is enhanced as a consequence of the increased amplitude and altered localization of their upstream stimulatory calcium signals. For example, adult ventricular myocytes express low levels of the inositol 1,4,5′-triphosphate II (IP_3RII) calcium channel within the membranes of the sarcoplasmic and perinuclear calcium stores at baseline (Lipp et al., 2000; Guatimosim et al., 2008; Luo et al., 2008; Higazi et al., 2009). However, in failing human myocardium and cardiomyocytes from genetic and experimentally induced animal models of hypertrophy, IP_3RII levels are increased (Harzheim et al., 2009, 2010; Nakayama et al., 2010). Under these conditions, IP_3-induced calcium release (IICR) from IP_3RII has deleterious effects on cellular function. Ectopic release of calcium from the sarcoplasmic reticulum has pro-arrhythmic properties (Harzheim et al., 2009), while IICR in the perinuclear region engages the activity of calcium-dependent transcriptional regulators, leading to the induction of pro-hypertrophic patterns of gene expression (Wu et al., 2006; Higazi et al., 2009; Guo et al., 2012). Intriguingly, we have previously reported that increased protein expression of IP_3RII during hypertrophy is not accompanied by an increase at the mRNA level (Harzheim et al., 2009), suggesting that receptor expression is up-regulated post-transcriptionally.

Notably, post-transcriptional regulatory mechanisms are known to fulfill a critical role in both cardiac development and disease (Small and Olson, 2011) and commonly involve the activity of micro-RNAs (miRNAs). miRNAs are small noncoding RNAs that influence gene expression by binding to sequences that include the 3′ untranslated region (3′UTR) of newly synthesized mRNA transcripts. As a result, protein expression from these transcripts is inhibited by mRNA degradation or translational repression (Bartel, 2004). The power of miRNA-mediated regulation of gene expression is illustrated by the observation that a single miRNA can target hundreds of mRNAs (Lim et al., 2005; Matkovich et al., 2011), providing a mechanism whereby a network of genes can be subject to coordinated and simultaneous regulation. Consequently, a change in the pattern of miRNAs expressed by a cardiomyocyte could generate genome-wide remodeling of gene expression and hence induce hypertrophy. Consistent with this hypothesis, miRNA expression is altered in a diagnostic manner in left ventricular samples taken from humans suffering from a variety of cardiac pathologies (Ikeda et al., 2007) and in mouse models of hypertrophic remodeling (van Rooij et al., 2006). More specifically, miRNAs including miR-1 (Sayed et al., 2007; Li et al., 2010b), miR-133a (Carè et al., 2007), and miR-208a (van Rooij et al., 2007) show altered expression in hypertrophy and have been directly implicated in induction of the hypertrophic response. These disease-associated profiles of miRNA expression are likely to be generated in response to hypertrophic stimuli by modification of miRNA transcription or processing mechanisms, elicited by the activity of intracellular signaling pathways. Defining precisely how miRNA expression and pro-hypertrophic pathways are interrelated is likely to provide important insight into the complexity of cardiomyocyte gene regulatory networks.

Here, we investigate the mechanisms that produce up-regulation of IP_3RII during hypertrophic cardiomyocyte remodeling, showing that decreased expression of miR-133a allows IP_3RII expression to increase, thereby promoting hypertrophy. Furthermore, by identifying that calcium released from IP_3RII suppresses miR-133a levels, we delineate a pro-hypertrophic positive feedback loop initiated and perpetuated by IICR.

Results

IP_3RII protein expression increases in the cardiomyocyte during pressure overload–induced hypertrophy

To examine the mechanisms responsible for increased IP_3-dependent signaling during pathological cardiac remodeling, we used an in vivo hypertrophy model. Aortic banding (AB) induces a pressure-overload hypertrophic response and eventual heart failure in adult rats, exemplified by an increase in the ratio of left ventricular weight to body weight (Fig. 1 a) and enhanced mRNA expression of the hypertrophic marker gene atrial natriuretic factor (ANF; Fig. 1 b). Echocardiography confirmed the presence of pathological left ventricular remodeling and contractile dysfunction (Fig. 1, c and d). Our previous observations have demonstrated an increase in IP_3RII protein expression that is restricted to the cardiomyocytes of the hypertrophic heart (Harzheim et al., 2009, 2010). This response is not recapitulated in the non-cardiomyocyte population, which expresses negligible amounts of IP_3RII protein under both control (Perez et al., 1997; Harzheim et al., 2010) and hypertrophic conditions (Harzheim et al., 2009, 2010). Consistent with these data, immunoblotting demonstrated that IP_3RII protein expression was increased in the AB samples (Fig. 1, e and f). Up-regulation of IP_3RII within the cardiomyocyte specifically was shown in immunofluorescence images of ventricular myocytes isolated from sham and AB rats (Fig. 1 g). Quantitation of the intensity and distribution of immunostained proteins by 2D Fourier analysis showed that expression of IP_3RII was increased in the AB samples, whereas RyR2 expression and distribution were unaltered (Fig. S1, a and b). Furthermore, the ratio of pixels positive for IP_3RII to RyR2 was increased in the hypertrophic myocytes (Fig. 1 h). Together, these data confirm that the increase in IP_3RII protein during hypertrophy is myocyte specific. Intriguingly, abundance of IP_3RII mRNA was unaltered (Fig. 1 i) and nascent IP_3RII RNA expression, a measure of transcriptional activity at the IP_3RII gene (*Itpr2*) locus, was decreased after AB (Fig. 1 j). Consequently, we considered a post-transcriptional regulatory mechanism to explain pro-hypertrophic IP_3RII up-regulation in the cardiomyocyte.

Published November 19, 2012

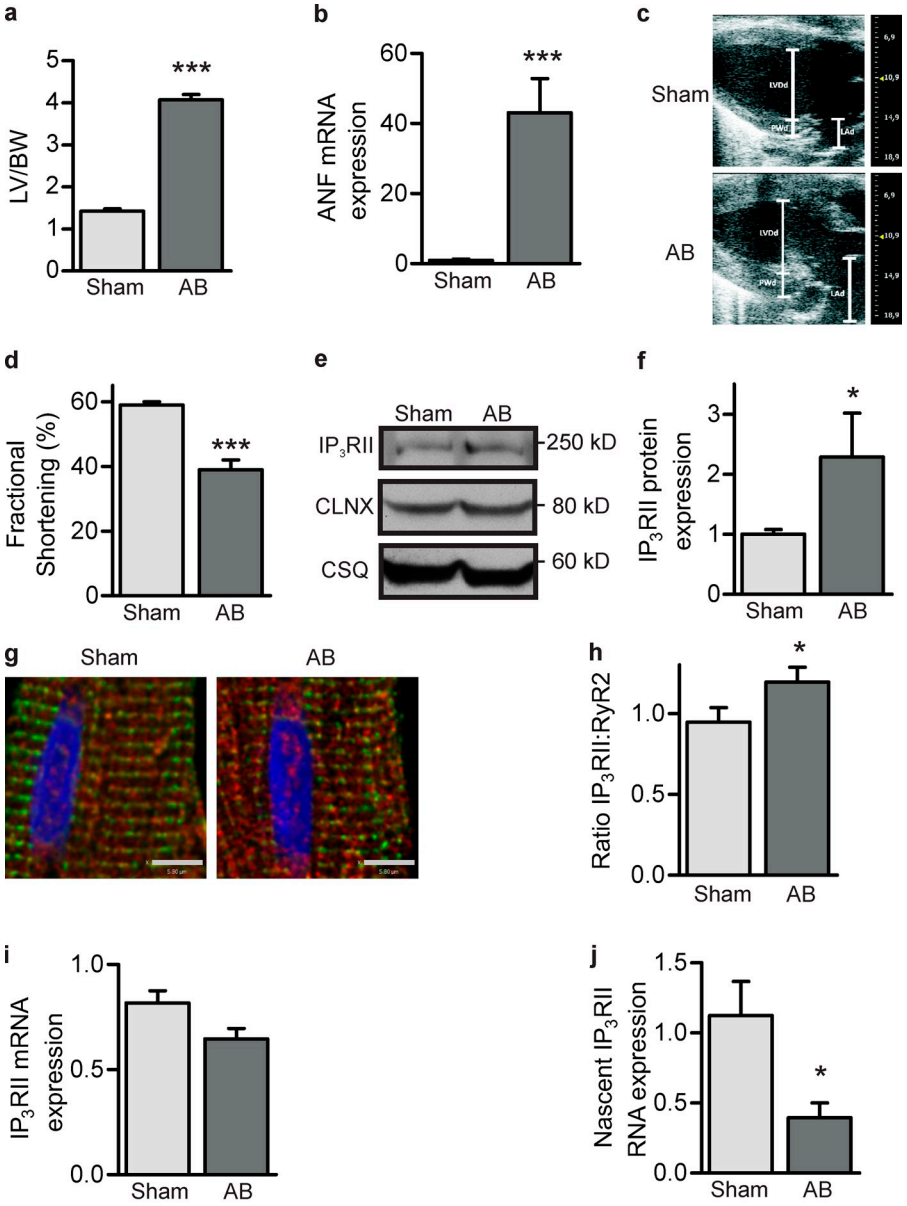

Figure 1. **IP_3RII is up-regulated post-transcriptionally during hypertrophy in cardiac myocytes.** (a) Quantification of the ratio of left ventricular weight to body weight in sham and AB adult rats. (b) Analysis of ANF mRNA expression by qPCR in sham and AB left ventricular samples. (c) Representative echocardiography of sham and AB rats. Dimensions indicate left ventricular diastolic dimension (LVDd) and posterior wall thickness (PWd), indices of ventricular function and hypertrophy, respectively. (d) Fractional shortening quantification (%) from echocardiographic analysis of eight sham and six AB rats. (e) Immunoblot for IP_3RII in the membrane protein fraction of sham and AB ventricular lysates. Calnexin (CLNX) and calsequestrin (CSQ) are shown as loading controls. (f) Quantification of immunoblots as in e; $n = 5$. (g) Immunofluorescence image of ventricular myocytes isolated from sham and AB rats. IP_3RII is shown in red, RyR2 in green, and DAPI in blue. Bar, 5.8 µm. (h) Ratio of IP_3RII to RyR2 quantified from immunofluorescence images as in g. For the sham condition, 16 cells from 2 independent preparations were analyzed. For the AB condition, 26 cells from 2 independent preparations were analyzed. (i) IP_3RII mRNA expression measured by qPCR in sham/AB samples. (j) Nascent IP_3RII RNA expression measured by qPCR in the sham/AB samples. Bar graphs are mean ± SEM from at least three independent experiments. *, $P < 0.05$; ***, $P < 0.001$.

IP_3RII expression is regulated by miR-133a

miRNAs are powerful mediators of post-transcriptional control of gene expression networks and have proven roles in cardiac development and disease (Small and Olson, 2011). To determine whether IP_3RII expression is regulated in this manner, we visually inspected the 3′UTR of the *Itpr2* gene for putative seed sequences for hypertrophy-related miRNAs. This analysis revealed a seed sequence for the anti-hypertrophic miRNA rno-miR-133a (Carè et al., 2007), which was conserved between rat, mouse, and human (Fig. 2 a). In view of this finding and previously published data that have demonstrated repression of miR-133a in hypertrophy (Carè et al., 2007), we measured miR-133a expression after AB. miR-133a levels were decreased in the AB samples (Fig. 2 b), thereby providing a potential mechanism for the increase in IP_3RII expression. The hypertrophy-associated decrease in miR-133a expression was specific to the cardiomyocyte population, as after AB, miR-133a expression in noncardiomyocytes was unchanged (Fig. S1 c). This result is in concordance with the observation that IP_3RII protein expression is unaltered in noncardiomyocytes under hypertrophic conditions (Harzheim et al., 2010), suggesting that miR-133a and IP_3RII expression levels may be inversely correlated. The genomic sequence encoding miR-133a is clustered bi-cistronically with the sequence for another muscle-specific miRNA, miR-1. Quantification of miR-1 levels in the AB samples demonstrated that expression of this miRNA is also decreased in hypertrophy (Fig. 2 c). However, as the *Itpr2* 3′UTR does not contain a seed sequence for miR-1, we chose to focus on regulation of IP_3RII expression by miR-133a in our subsequent experiments.

Hence, to verify that IP_3RII mRNA is a bona fide target for miR-133a, we analyzed the activity of a luciferase reporter that tests for miRNA regulation of potential target sequences. In this reporter, the 3′UTR of the *Itpr2* was inserted downstream of constitutively expressed luciferase (Fig. 2 d). As a control, the putative miR-133a seed sequence within the *Itpr2* 3′UTR

Published November 19, 2012

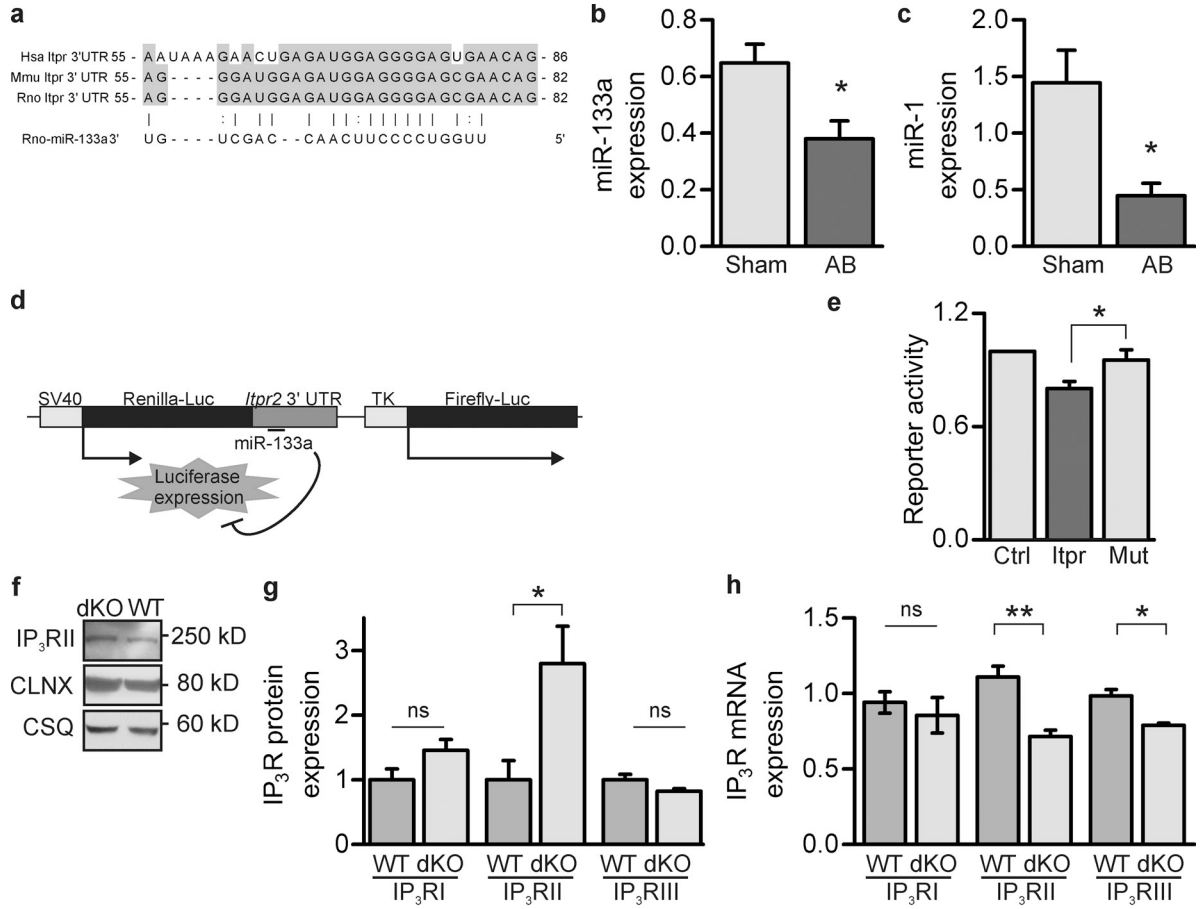

Figure 2. **miR-133a regulates IP_3RII expression.** (a) Conservation of the miR-133a seed sequence between the human, mouse, and rat *Itpr2* 3′UTR. (b) miR-133a expression in sham and AB samples measured by qPCR. (c) miR-1 expression in sham and AB samples. (d) Schematic representation of the luciferase reporter construct used to measure miR-133a repressive activity at the *Itpr2* 3′UTR. (e) Luciferase activity in HEK293 cells transfected with miR-133a and either the *Itpr2* 3′UTR reporter or mut-*Itpr2* 3′UTR reporter. (f) Immunoblot for IP_3RII in left ventricular samples from wild-type (WT) or miR-133a-1, miR-133a-2 double knockout mice (dKO). (g) Quantification of immunoblots for $IP_3RI/II/III$ from WT/dKO samples as in f; $n = 6$. (h) $IP_3RI/II/III$ mRNA expression in samples as in f. Bar graphs represent the mean ± SEM from at least three independent experiments. *, $P < 0.05$; **, $P < 0.01$.

was mutated to prevent miR-133a association. Co-transfection of the luciferase reporters and a miR-133a expression plasmid into HEK293 cells revealed that luciferase activity was decreased by the wild-type *Itpr2* 3′UTR but not the mutant *Itpr*2 3′UTR (Fig. 2 e). Therefore, the *Itpr*2 3′UTR contains a functional miR-133a binding site. To substantiate these results, we analyzed IP_3RII protein and mRNA expression in ventricular samples from miR133a-1, miR133a-2 double-knockout mice (Fig. 2, f–h; Liu et al., 2008). In the absence of miR-133a, IP_3RII protein levels were increased (Fig. 2, f and g) while IP_3RII mRNA expression was diminished (Fig. 2 h). Together, these data confirm that miR-133a regulates IP_3RII post-transcriptionally. Although the 3′UTRs of *Itpr1*and *Itpr3* do not contain seed sequences for miR-133a, the abundance of their protein products was also examined. Expression of IP_3RI and IP_3RIII were unaltered in the hearts of knockout animals (Fig. 2 g), confirming that these receptor isoforms are not a target for miR-133a and that up-regulation of IP_3 receptors is not a general consequence of the miR-133a knockout phenotype. Together, these results imply that lack of miR-133a–mediated repression during hypertrophy augments IP_3RII protein expression.

miR-133a overexpression decreases IP_3RII protein levels

To dissect the mechanisms underlying miR-133a regulation of the IP_3RII, we conducted experiments using primary cultures of neonatal rat ventricular myocytes (NRVMs). First, we increased miR-133a expression using an adenoviral approach. miR-133a overexpression was confirmed by quantitative real-time PCR (qPCR; Fig. 3 a) and viral infection was monitored by the presence of coexpressed GFP (Fig. 3 b). In concordance with our hypothesis, miR-133a–overexpressing myocytes exhibited decreased IP_3RII expression when compared with control myocytes (Fig. 3, c and d). These data indicate that increasing miR-133a down-regulates IP_3RII.

Inhibition of miR-133a elicits IICR-dependent hypertrophic remodeling

To further establish the effect of miR-133a upon IP_3RII expression, we inhibited miR-133a binding to its targets by antagomir transfection. In the presence of the antagomir, basal levels of the IP_3RII were increased and the repressive effect of miR-133a overexpression was prevented (Fig. 3 e). This result indicates that under nonstimulated conditions in NRVMs, miR-133a

Published November 19, 2012

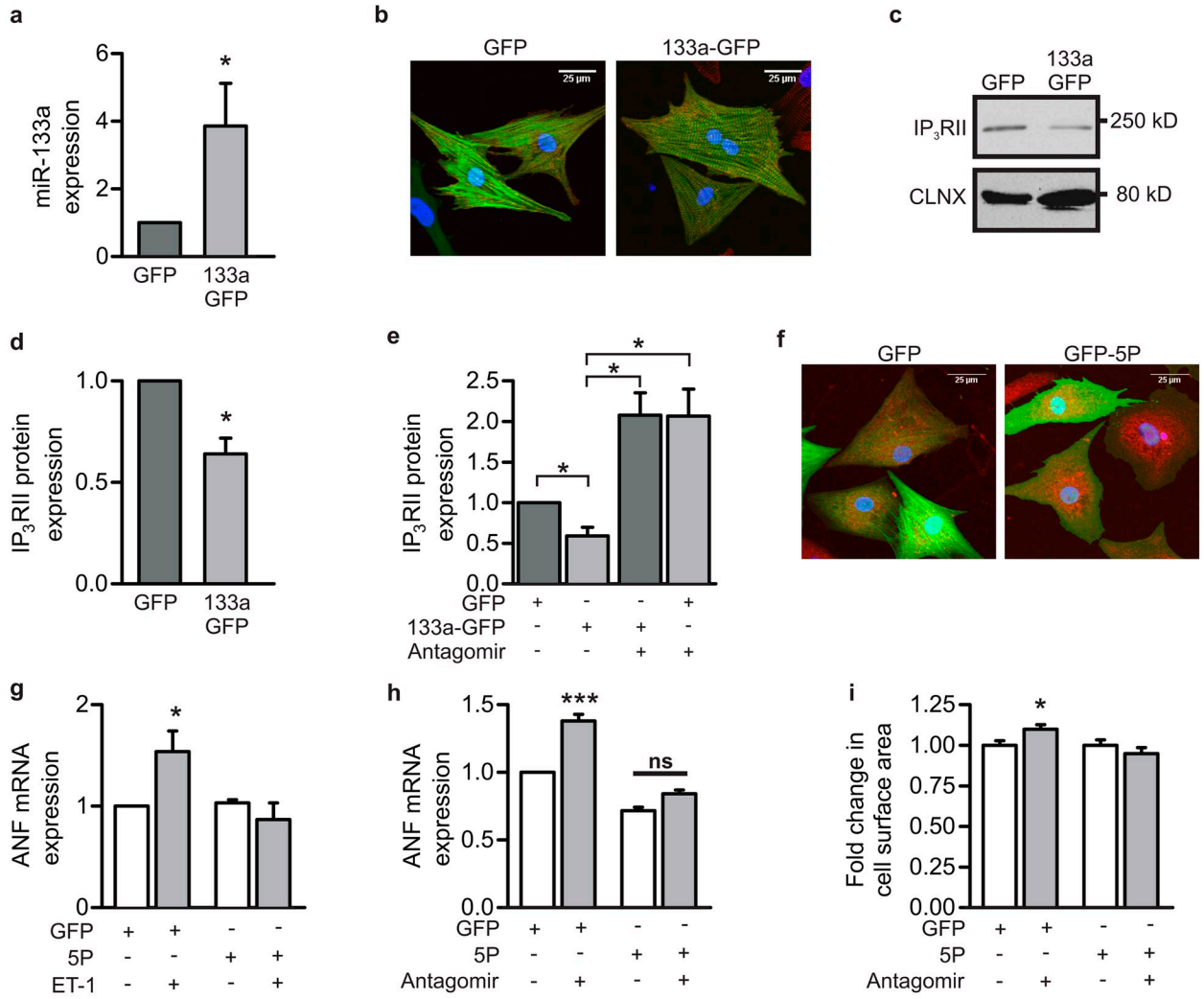

Figure 3. **miR-133a inhibits IP_3RII expression restraining pro-hypertrophic IICR.** (a) Overexpression of miR-133a-GFP in neonatal rat ventricular myocytes (NRVMs) quantified by qPCR. (b) Immunofluorescence image of NRVMs expressing GFP/GFP-miR-133a. GFP is shown in green, α-actinin in red, and DAPI in blue. (c) Immunoblot for IP_3RII in GFP/GFP-miR-133a overexpressing NRVMs. (d) Quantification of immunoblots from samples as in c; $n = 8$. (e) IP_3RII expression measured by immunoblotting ($n = 6$) in NRVMs transfected with a control oligo or miR-133a–specific antagomir and infected with GFP/GFP-miR-133a. (f) Immunofluorescence image of NRVMs expressing GFP/GFP-5P. GFP is shown in green, α-actinin in red, and DAPI in blue. (g) ANF mRNA expression in NRVMs expressing GFP/GFP-5P and treated with 100 nM endothelin-1 (ET-1) for 24 h. (h) ANF mRNA expression in NRVMs transfected with control/miR-133a–specific antagomir and infected with GFP/GFP-5P. (i) Cell surface area quantification in NRVMs transfected and infected as in h. Data are mean ± SEM from at least three independent experiments.*, $P < 0.05$; ***, $P < 0.001$.

restrains IP_3RII expression. Because IICR from IP_3RII is an important inducer of hypertrophic remodeling (Higazi et al., 2009; Nakayama et al., 2010), we next hypothesized that the increased IP_3RII expression resulting from antagomir transfection contributes to the pro-hypertrophic effect of miR-133a inhibition. To test this hypothesis, we investigated whether suppression of IICR in NRVMs prevents the hypertrophic remodeling induced by miR-133a antagomir (Fig. 3 f). Confirming the dependence of the hypertrophic response on IICR and as we have previously described, adenoviral overexpression of GFP-tagged type 1 IP_3 5′-phosphatase (GFP-5P) suppressed the induction of ANF mRNA expression elicited by the pro-hypertrophic agonist endothelin-1 (ET-1; Fig. 3 g; Higazi et al., 2009; Drawnel et al., 2012). We next examined the effect of GFP-5P inhibition of IICR upon miR-133a antagomir-induced hypertrophic remodeling. Consistent with the anti-hypertrophic role of miR-133a, ANF mRNA expression and cell surface area were increased in NRVMs transfected with the miR-133a antagomir (Fig. 3, h and i). Notably, in the presence of GFP-5P, antagomir transfection did not elicit an increase ANF mRNA expression (Fig. 3 h) or cell surface area (Fig. 3 i), indicating that IICR is required for the pro-hypertrophic effect of antagomir transfection. More significantly, these results suggest that when miR-133a activity is decreased, as is observed during hypertrophy in vivo (Fig. 1), IP_3RII expression increases and can initiate IICR-dependent cellular remodeling.

Basal IP_3RII expression is restricted by miR-133a

As miRNAs can target multiple different mRNAs (Bartel and Chen, 2004), a direct link between miR-133a, IP_3RII, and hypertrophy was lacking. To establish such a link, we transfected

Published November 19, 2012

a target protector (TP) oligonucleotide designed to specifically protect the *Itpr2* 3′UTR from miR-133a without affecting other miR-133a targets (Choi et al., 2007). TP transfection resulted in increased IP_3RII abundance compared with control TP (Fig. 4 a), whereas expression of another miR-133a target, serum response factor (SRF; Liu et al., 2008), was unaltered. The *Itpr2* miR-133a site-specific TP-induced increase in IP_3RII expression was also observed in experiments in which oligonucleotides targeting regions of the *Itpr2* 3′UTR proximal to but not overlapping with the miR-133a seed sequence were used instead of the manufacturer's control for transfection. This indicates that the effect of the TP was due to inhibition of miR-133a binding to the *Itpr2* 3′UTR rather than disruption of the *Itpr2* 3′UTR structure (Fig. S2). Moreover, in cells transfected with these control TPs, SRF expression was unaltered (Fig. S2). Thus, by preventing miR-133a binding, the IP_3RII TP specifically induces IP_3RII up-regulation, in the absence of changes in the expression of other targets of miR-133a. Using this approach allows the specific role of miR-133a–mediated regulation of IP_3RII expression in the cardiomyocyte to be interrogated. Therefore, we examined whether preventing miR-133a–mediated IP_3RII repression by TP transfection is sufficient to induce hypertrophic remodeling. Indeed, baseline expression of the hypertrophic marker ANF and cell surface area were increased in NRVMs transfected with the IP_3RII TP (Fig. 4, b and c), confirming that the cardiomyocyte hypertrophic response is restricted by the inhibitory effect of miR-133a on the IP_3RII. Therefore, when miR-133a–mediated IP_3RII repression is removed, a hypertrophic phenotype develops.

miR-133a–mediated regulation of IP_3RII controls IICR and hypertrophic gene expression

We extended our studies regarding the role of miR-133a–mediated suppression of IP_3RII to the adult rat ventricular myocyte (ARVM), giving particular consideration to calcium homeostasis and hypertrophic remodeling. At baseline, ARVMs express a low level of IP_3RII. Under conditions of ryanodine-receptor inhibition, these receptors produce calcium puffs when stimulated with cell-permeant IP_3-ester (Tovey et al., 2001; Berridge et al., 2003; Harzheim et al., 2009). We aimed to repress IP_3RII expression and consequently IICR by increasing miR-133a activity using adenovirus. miR-133a overexpression and the associated down-regulation of IP_3RII were confirmed by qPCR (Fig. S3 a) and immunoblotting (Fig. S3 b), respectively. We then assessed the effect of increased miR-133a on IP_3RII function in control and miR-133a–overexpressing ARVMs. Fluo-4–loaded cells were acutely treated with tetracaine to block the ryanodine receptor, while the IP_3RII was stimulated with IP_3-ester. When miR-133a was overexpressed, IP_3-ester elicited significantly fewer calcium release events (Fig. 4 d), an effect that correlates with reduced IP_3RII expression.

As IP_3-dependent calcium signals promote hypertrophic gene expression (Wu et al., 2006; Higazi et al., 2009; Nakayama et al., 2010), we next examined whether miR-133a overexpression is sufficient to modulate the hypertrophic phenotype both in vitro and in vivo. First, we used the spontaneously hypertensive rat (SHR) model of cardiac hypertrophy. These animals have a disease progression that closely mirrors that observed in human patients (Dillmann, 2008), as they develop hypertension, cardiac hypertrophy, and heart failure with increasing age. As observed in hearts from AB rats, isolated hypertrophic adult SHR myocytes exhibited an increase in IP_3RII protein expression, unaltered IP_3RII RNA levels (Fig. 4 e), and decreased expression of miR-133a (Fig. 4 f) when compared with the Wistar Kyoto (WKY) control. Befitting their hypertrophic status, ANF expression was increased in SHR myocytes (Fig. 4 g). Upon miR-133a overexpression, ANF expression returned to the control level (Fig. 4 g), indicating regression of the hypertrophic phenotype.

To establish a link between miR-133a–mediated regulation of IP_3RII and hypertrophic remodeling in vivo, we analyzed mice infused via an osmotic mini-pump for 1 mo with saline or a miR-133a–specific antagomir oligo (Carè et al., 2007). It has been previously reported that inhibition of the activity of miR-133a by antagomir infusion elicits a hypertrophic response (Carè et al., 2007). This was exemplified by increased diastolic left ventricular posterior wall dimension (LVPWd) in the antagomir-treated mice (Fig. 4 h). Therefore, in the absence of miR-133a, hypertrophy is induced. Consistent with its role in hypertrophic remodeling, IP_3RII protein expression was enhanced under antagomir-treated conditions (Fig. 4, i and j). Comparison of IP_3RII protein levels in control mice and mice infused with a scrambled miR-133a antagomir revealed that IP_3RII expression was unaffected by the scrambled oligonucleotide (Fig. S4, a and b). Hence, up-regulation of IP_3RII is a specific effect of the miR-133a antagomir. Taken with the data arising from miR-133a inhibition/overexpression in neonatal and adult cardiomyocytes in vitro (Fig. 4, b, c, and g), these results demonstrate that miR-133a inhibits IP_3RII expression in ventricular myocytes, restraining pro-hypertrophic IICR and preventing hypertrophic remodeling of the heart.

Transcription of miR-133a is regulated by an IICR-dependent mechanism

Thus far, we have demonstrated that the expression patterns of IP_3RII and miR-133a are inversely correlated in the cardiomyocyte and that miR-133a restrains pro-hypertrophic IICR. However, the mechanism whereby miR-133a levels are diminished during hypertrophy is unclear. Previously, we and others have shown that calcium release via IP_3RII regulates pro-hypertrophic transcription (Higazi et al., 2009; Nakayama et al., 2010). We investigated whether the hypertrophy-associated decrease in miR-133a expression is produced by transcriptional inhibition and whether the mechanism of miR-133a repression relies on IICR. First, we measured expression of miR-133a in NRVMs treated with ET-1 to determine whether the response to ET-1 can be used to study mechanisms of miR-133a suppression. ET-1 stimulation decreased expression of mature miR-133a (Fig. 5 a) and increased levels of IP_3RII protein. Overexpression of miR-133a prevented the ET-1–induced increase in IP_3RII (Fig. 5 b), which would be anticipated given that miR-133a suppresses IP_3RII. As calcium released from IP_3RII induces hypertrophic gene expression, induction of the hypertrophic marker gene

Published November 19, 2012

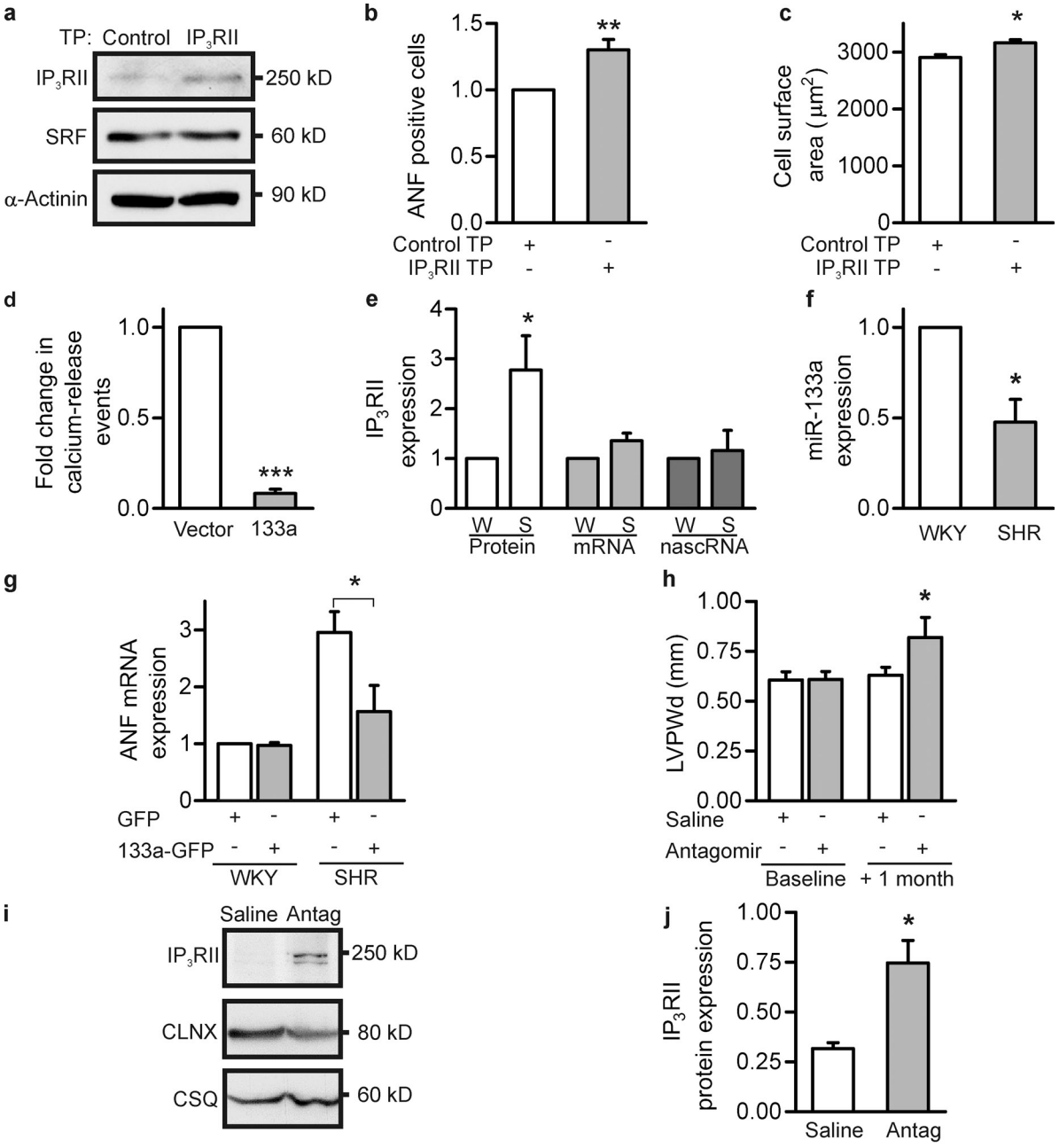

Figure 4. **Antagonism of miR-133a–mediated regulation of IP_3RII induces the hypertrophic response.** (a) Immunoblot for IP_3RII and SRF in NRVMs transfected with control or IP_3RII-specific target protector (TP) oligos. α-Actinin is shown as a loading control. (b) ANF protein expression in NRVMs transfected as in a. (c) Cell surface area measurements of NRVMs transfected as in panel a. More than 500 cells were measured per condition. (d) Quantification of the fold change in the number of calcium release events elicited by IP_3-ester in ARVMs infected with control or miR-133a adenovirus. For each condition, at least eight ARVMs were analyzed from three separate experiments. (e) IP_3RII protein, mRNA, and nascent RNA expression in WKY and SHR myocytes measured by immunoblotting or qPCR. (f) miR-133a expression analyzed by qPCR in WKY/SHR myocytes. (g) Quantification of the hypertrophic phenotype by measurement of ANF mRNA expression in GFP/miR-133a-GFP overexpressing WKY and SHR ventricular myocytes. (h) Measurement of LVPWd by echocardiography in mice at baseline and after infusion with saline or miR-133a antagomir for 1 mo. (i) Immunoblot for IP_3RII in left ventricular samples from mice treated with saline/antagomir for 1 mo. (j) Quantification of immunoblots as in i; $n = 3$. Bar graphs are mean ± SEM from at least three independent experiments. *, $P < 0.05$; ***, $P < 0.001$.

ANF in response to ET-1 was also prevented by miR-133a overexpression (Fig. 5 c). These data are consistent with the results from the in vivo models of hypertrophy, validating the use of ET-1–treated NRVMs to investigate miR-133a repression. Next, we tested whether the ET-1–induced reduction in miR-133a has a transcriptional mechanism of origin by quantifying expression of primary miR-133a (primiR-133a). Interestingly, primiR-133a levels were significantly decreased upon ET-1 stimulation (Fig. 5 d), showing that reduced transcription rather than altered processing mediates the hypertrophy-associated decrease in miR-133a.

As pro-hypertrophic transcriptional activity is regulated by IICR (Wu et al., 2006; Higazi et al., 2009; Nakayama et al., 2010), we examined whether this signaling pathway participates

Published November 19, 2012

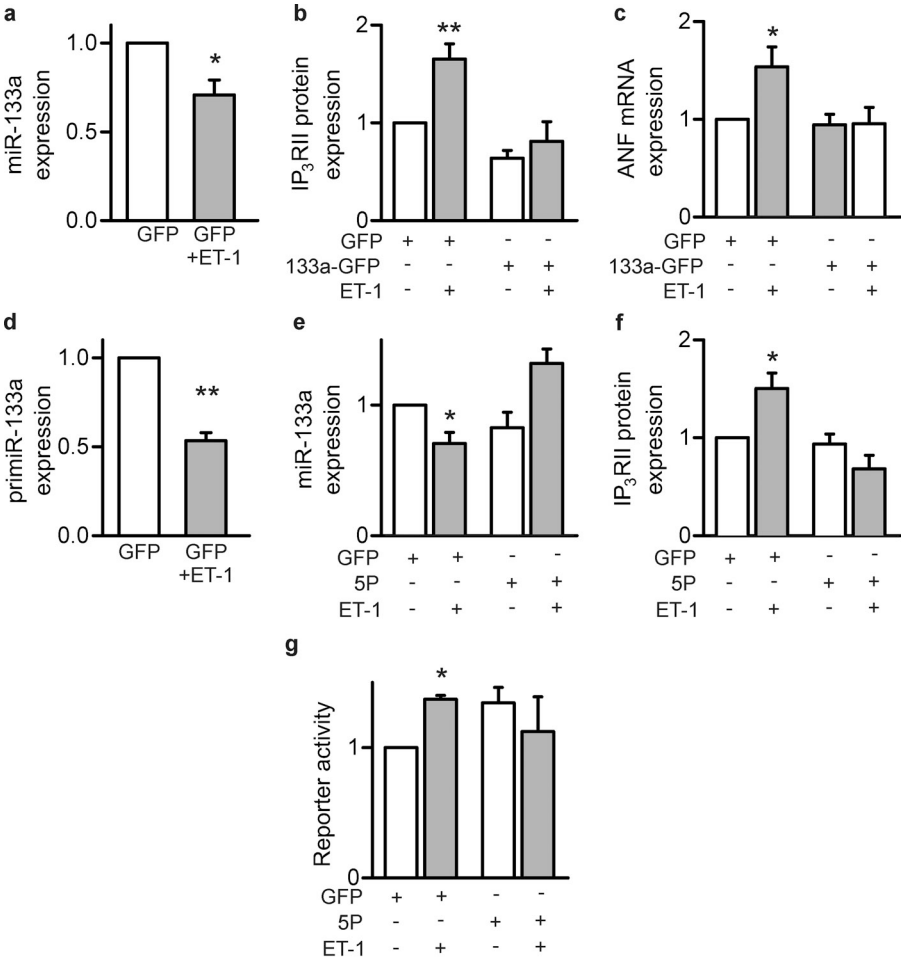

Figure 5. **IICR is required for decreased miR-133a expression during hypertrophy.** (a) miR-133a expression measured by qPCR in NRVMs stimulated with 100 nM endothelin-1 (ET-1) for 24 h. (b) Immunoblot analysis to quantify IP_3RII protein expression in GFP/miR-133a-GFP overexpressing NRVMs cultured in the presence and absence of ET-1 for 24 h. Seven independent immunoblots were quantitated. (c) qPCR analysis of the hypertrophic response to ET-1 in GFP/miR-133a-GFP overexpressing NRVMs by quantification of ANF mRNA expression. (d) Transcriptional activity at the miR-133a locus was measured by qPCR quantification of primiR-133a levels in control and ET-1-treated NRVMs. e. Measurement of miR-133a expression by qPCR in NRVMs infected with GFP/GFP-5P and treated with ET-1 for 24 h. (f) IP_3RII protein expression assessed by immunoblotting of NRVM lysates treated as in e. At least four blots were quantitated per condition. (g) Luciferase assay of NRVMs transfected with the *Itpr2* 3′UTR reporter construct, infected with either GFP or GFP-5P and treated with ET-1 for 24 h. Data are mean ± SEM from at least three independent experiments. *, $P < 0.05$; **, $P < 0.01$.

in miR-133a repression. To this end, IICR was inhibited in NRVMs by GFP-5P overexpression (Fig. 3 f), and the effect of this manipulation on the ET-1–stimulated decrease in miR-133a quantitated. GFP-5P prevented both the ET-1–stimulated decrease in miR-133a (Fig. 5 e) and increase in IP_3RII protein expression (Fig. 5 f). These data imply that IICR is required for ET-1–induced repression of miR-133a expression and the resulting up-regulation of IP_3RII. Therefore, by diminishing miR-133a expression, IICR enhances expression of its source calcium channel. We further substantiated this hypothesis by using the *Itpr2* 3′UTR reporter construct (Fig. 2 d) to more directly measure the repressive action of miR-133a on the *Itpr2* 3′UTR. Activity of this reporter was increased in NRVMs treated with ET-1 (Fig. 5 g), reflecting the ET-1–induced decrease in miR-133a. In cells overexpressing GFP-5P, ET-1 did not elicit a change in reporter activity, supporting a mechanism whereby IICR diminishes miR-133a levels. Together, these data suggest an intriguing hypothesis, whereby increases in IP_3RII expression would create a positive feedback loop to further increase IICR, driving miR-133a down-regulation and the hypertrophic response. Having demonstrated in NRVMs that IICR controls IP_3RII expression through modulation of miR-133a levels, we next determined whether this mechanism is conserved in vivo. Consequently, we examined miR-133a expression in IP_3RII-transgenic mice (Fig. 6 a), which exhibit enhanced IICR and spontaneous mild hypertrophy at 3 mo of age (Nakayama et al., 2010). We also investigated the effect of thoracic aortic constriction (TAC) on these mice. In control mice expressing the tetracycline transactivator (tTA) alone, TAC induced a decrease in miR-133a expression (Fig. 6 b) and an increase in IP_3RII protein expression (Fig. 6 c). At baseline, miR-133a expression was lower in IP_3RII-TG mice, with no further decrease produced upon TAC (Fig. 6 b). These data support the hypothesis that IICR is a key initiating signal, which suppresses miR-133a and induces hypertrophy. Interestingly, IP_3RII overexpression did not elicit a similar decrease in miR-1 expression (Fig. S5 a), suggesting that the IICR-mediated signal has a specific effect on miR-133a.

Next, we performed the converse experiment, examining the effect of inhibition of IICR upon miR-133a and IP_3RII levels in vivo. To this end, we used mice engineered to inducibly express the IP_3-sponge, a fragment of IP_3RI spanning its ligand-binding domain that binds free IP_3 with very high affinity (Uchiyama et al., 2002; Nakayama et al., 2010). These mice show blunted hypertrophic responses to systemic infusion with the hypertrophic agonists angiotensin II and isoproterenol (Nakayama et al., 2010). IP_3-sponge mice demonstrated elevated baseline miR-133a expression when compared with tTA mice (Fig. 6 d) and no significant change in miR-1 expression (Fig. S5 b). There was no difference in IP_3RII protein expression

Published November 19, 2012

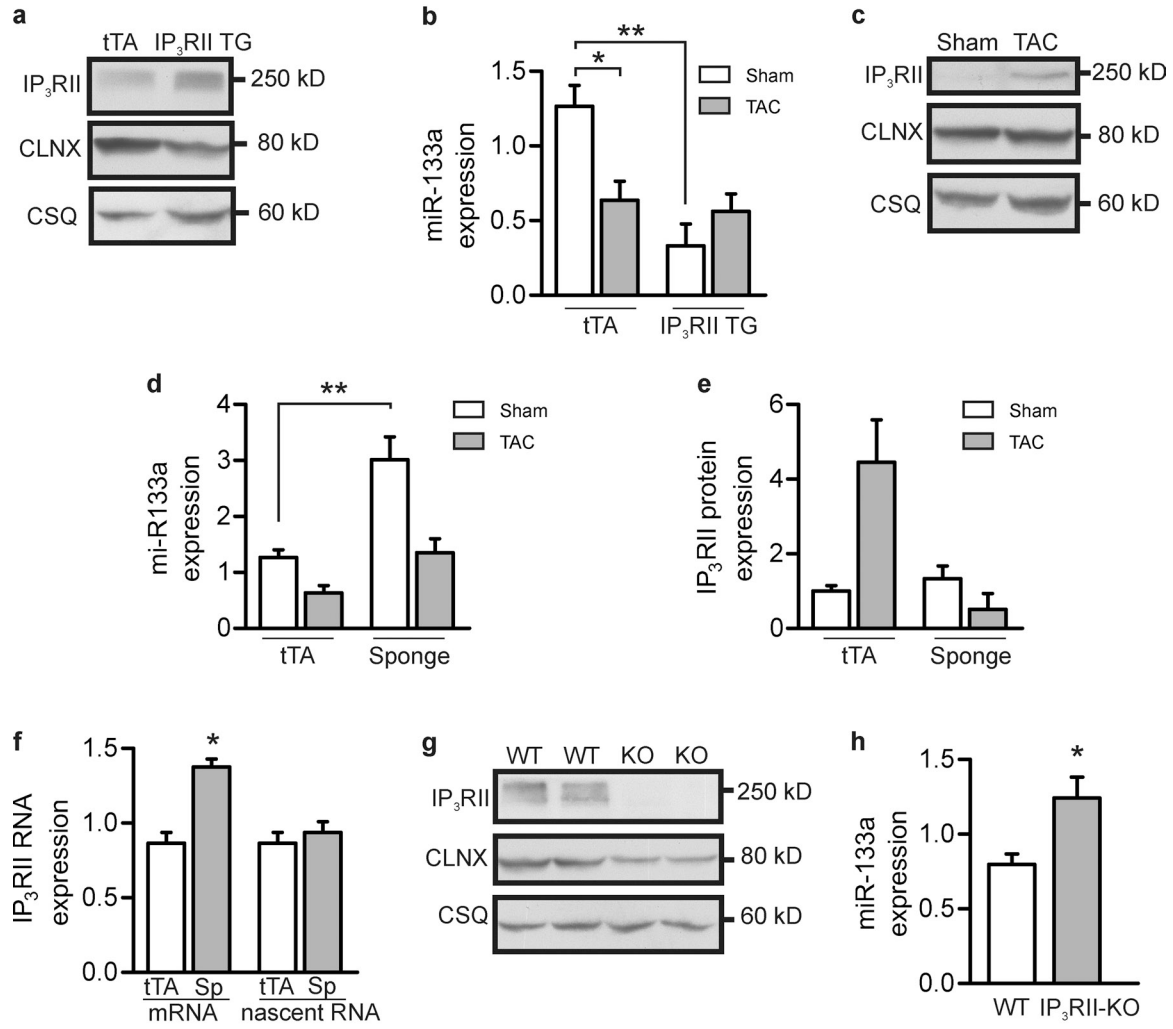

Figure 6. **Manipulation of IICR in vivo alters miR-133a expression.** (a) Immunoblot for IP_3RII in left ventricular lysates from IP_3RII transgenic mice. Tetracycline transactivator protein (tTA) mice are used as controls. (b) miR-133a expression measured by qPCR in tTA/IP_3RII transgenic mice subjected to sham or TAC procedures. For the tTA sham/TAC and IP_3RII-TAC conditions, three mice were analyzed. For the IP_3RII-sham condition, two mice were analyzed. (c) Representative immunoblot for IP_3RII in tTA ventricular lysates ± TAC. (d) qPCR analysis of miR-133a expression in ventricular lysates from tTA controls and IP_3-sponge (sponge) expressing mice subjected to sham or TAC procedures. For the tTA sham/TAC and IP_3-sponge-TAC conditions, three mice were analyzed. For the sponge-sham condition, two mice were analyzed. (e) Quantification of immunoblots for IP_3RII from sham or TAC operated tTA and sponge mice. Two mice were analyzed for the tTA-sham and sponge-sham conditions. Three mice were analyzed for the tTA-TAC and sponge-TAC conditions. (f) qPCR measurement of IP_3RII mRNA and nascent RNA expression in tTA and sponge mice. Three mice were analyzed for the tTA condition, two mice were analyzed for the sponge condition. (g) Example immunoblot of ventricular lysates from wild-type (WT) and IP_3RII knockout (KO) mice. (h) miR-133a expression measured using qPCR in four WT and four KO mouse samples. Bar graphs show mean ± SEM. *, $P < 0.05$; **, $P < 0.01$.

between IP_3-sponge mice and tTA control mice (Fig. 6 e), which is surprising given the alteration in miR-133a expression levels. However, analysis of IP_3RII RNA levels in the IP_3-sponge mice revealed increased IP_3RII mRNA, without a change in nascent RNA (Fig. 6 f). These data are suggestive of an adaptive mechanism, whereby increased stability of the IP_3RII mRNA transcript allows IP_3RII protein levels to be maintained. After TAC, miR-133a expression in the IP_3-sponge mice decreased to the baseline level observed in the control sham-operated tTA mice (Fig. 6 d), without producing an increase in IP_3RII expression (Fig. 6 e). This is not surprising given that miR-133a levels were the same as those observed in control animals. These data suggest that miR133a expression must fall below a threshold level before IP_3RII expression can increase and that in the absence of IICR, the threshold cannot be breached by hypertrophic stimulation. To examine the relationship between miR-133a and IICR using an alternative strategy, we analyzed samples from IP_3RII knockout mice (Fig. 6 g; Futatsugi et al., 2005). miR-133a expression was significantly increased when the IP_3RII was absent (Fig. 6 h), whereas miR-1 levels were unaltered (Fig. S5 c), mirroring the results observed in IP_3-sponge mice. Taken together, the in vitro and in vivo data indicate that IICR specifically controls expression of miR-133a. Enhanced IICR decreases miR-133a expression, whereas inhibition of IICR increases miR-133a.

Reduced SRF activity contributes to IICR-dependent miR-133a suppression

Although our results demonstrate a role for IICR in regulation of miR-133a, a remaining question concerns the mechanism(s)

Published November 19, 2012

by which IICR signals can repress primiR-133a transcription. It is known that the transcriptional regulator SRF targets the miR-133a locus (Zhao et al., 2005) and it has also been reported to inhibit synthesis of the primary miRNA transcript (Zhang et al., 2011). Thus, we tested whether SRF was involved in IICR-mediated regulation of miR-133a expression. Using a SRF-sensitive luciferase reporter, we determined that ET-1 stimulates SRF transcriptional activity in an IICR-dependent manner in NRVMs (Fig. 7 a). Furthermore, ET-1 also up-regulated SRF protein levels (Fig. 7, b and c), which is unsurprising given that SRF is a known miR-133a target (Liu et al., 2008). To address whether SRF has a role in regulation of miR-133a expression, we used an adenovirus to overexpress SRF and siRNA to reduce SRF expression (Fig. 7, d and e). SRF overexpression increased miR-133a (Fig. 7 f), decreased IP_3RII protein (Fig. 7, g and h), and was without effect on IP_3RII mRNA/nascent RNA expression (Fig. 7 i), indicating a lack of effect of SRF on *Itpr2* transcription. Conversely, SRF knockdown increased IP_3RII protein expression (Fig. 7, g and h). These results are consistent with a mechanism whereby SRF positively regulates miR-133a expression. However, SRF expression and activity are increased under hypertrophic stimulation, when miR-133a is down-regulated, suggesting a more complex interplay between miR-133a and SRF. This was further illustrated through the use of adenovirus to overexpress a dominant-negative (DN) form of SRF. DN-SRF lacks part of the transcription transactivation domain of SRF but retains the DNA-binding activity of the full-length protein (Belaguli et al., 1999). By binding to SRF target sequences while being unable to activate transcription, overexpression of the mutant has a dominant-negative effect on the activity of endogenous SRF. When DN-SRF was overexpressed, baseline miR-133a expression decreased (Fig. 7 j). This result supports the observation that under nonstimulated conditions, SRF activity drives miR-133a expression. DN-SRF prevented a further decrease in miR-133a expression after ET-1 treatment, implying that the repressive effect of pro-hypertrophic stimulation is mediated through inhibition of SRF transcriptional activity at the miR-133a loci.

The ability of SRF to regulate transcription in either an activating or repressive manner is determined by which of its many interacting proteins it is associated with (Posern and Treisman, 2006). We suggest that IICR promotes miR-133a suppression by altering the interaction and/or activity of one or more of these cofactors with SRF, leading to repression of SRF activity. One such protein is the homeodomain-only protein (HOP), which negatively regulates SRF-dependent transcriptional responses by recruiting class I HDACs (Kook et al., 2003). Hence, we next tested whether overexpression of HOP by adenoviral infection could mimic the effects of ET-1. miR-133a levels were diminished in HOP-overexpressing NRVMs, with ET-1 failing to elicit a further decrease (Fig. 7 k). In agreement with the reduced level of miR-133a, HOP overexpression increased baseline cell surface area (Fig. 7 l), indicative of hypertrophy. These findings support the notion that the inhibitory effect of ET-1 on miR-133a expression is mediated via a repressive transcription factor such as HOP, thus promoting development of a hypertrophic response. Further strengthening these observations, we demonstrate that HDAC activity is required for the ET-1–stimulated decrease in miR-133a. HDAC inhibition with trichostatin A (TsA) increased basal levels of miR-133a (Fig. 7 m) and prevented the inhibitory effect of ET-1 on miR-133a expression. As has been previously reported (Cao et al., 2011), TsA also prevented the ET-1–induced increased in ANF expression, confirming the role of HDACs in regulation of hypertrophic gene expression (Fig. 7 n).

Discussion

This study delineates an anti-hypertrophic role for miR133a that is intrinsic to the ventricular myocyte (Fig. 8). We show that in cardiomyocytes, the inhibitory action of miR-133a maintains low basal IP_3RII expression. Consequently, miR-133a activity holds IICR in check and the pro-hypertrophic effect of this pathway is restrained. This maintains an appropriate level of myocyte growth until the balance between miR-133a and IP_3RII is perturbed by pathological stimuli that elicit IICR. When IICR is engaged in this manner, miR-133a is suppressed via changes in SRF transcriptional activity/targeting. Hence, IP_3RII expression increases. A deleterious positive feedback loop is generated because enhanced IICR promotes sustained repression of miR-133a, providing a powerful driving force for pathological remodeling. Consequently, by inhibiting IP_3RII expression and IICR, miR-133a would be expected to prevent IICR-dependent pro-hypertrophic transcriptional responses.

By specific suppression of miR-133a, calcium arising from IP_3RII increases expression of its source channel, thereby amplifying the intensity of the pro-hypertrophic calcium signal. This creates an inherently unstable system whereby enhanced IICR serves to continually repress miR-133a and persistently increase IP_3RII expression. Interestingly, other pro-hypertrophic positive feedback loops have been identified involving miRNAs and the signaling pathways that regulate their expression. These include miR-1–dependent modulation of insulin-like growth factor-1 signaling (Elia et al., 2009) and miR-199b–mediated regulation of the NFAT negative regulatory kinase dual-specificity tyrosine phosphorylation–regulated kinase 1a (da Costa Martins et al., 2010). When taken together, these results indicate that several reciprocal regulatory loops may be active within the myocardium under pro-hypertrophic conditions. The self-perpetuating nature of these loops could serve to produce a sufficiently powerful and prolonged stimulus to induce genome-wide remodeling of gene expression and hence hypertrophic growth, overcoming mechanisms of negative regulation. The significance of a control loop involving miR-133a within this network is increased when collective consideration is given to the postulated targets of this miRNA. We have demonstrated regulation of IP_3RII, while other studies show repression of CnA (Dong et al., 2010) and NFATc4 (Li et al., 2010a). By targeting the IICR–Cn–NFAT pathway at multiple levels, miR-133a is an effective brake on pro-hypertrophic transcription. Consequently, when miR-133a levels decline in response to IICR, the source of activating calcium (IP_3RII), transducing mechanism (CnA), and effector (NFATc4) of the pathway are all up-regulated and pathological gene expression would be strongly promoted.

Published November 19, 2012

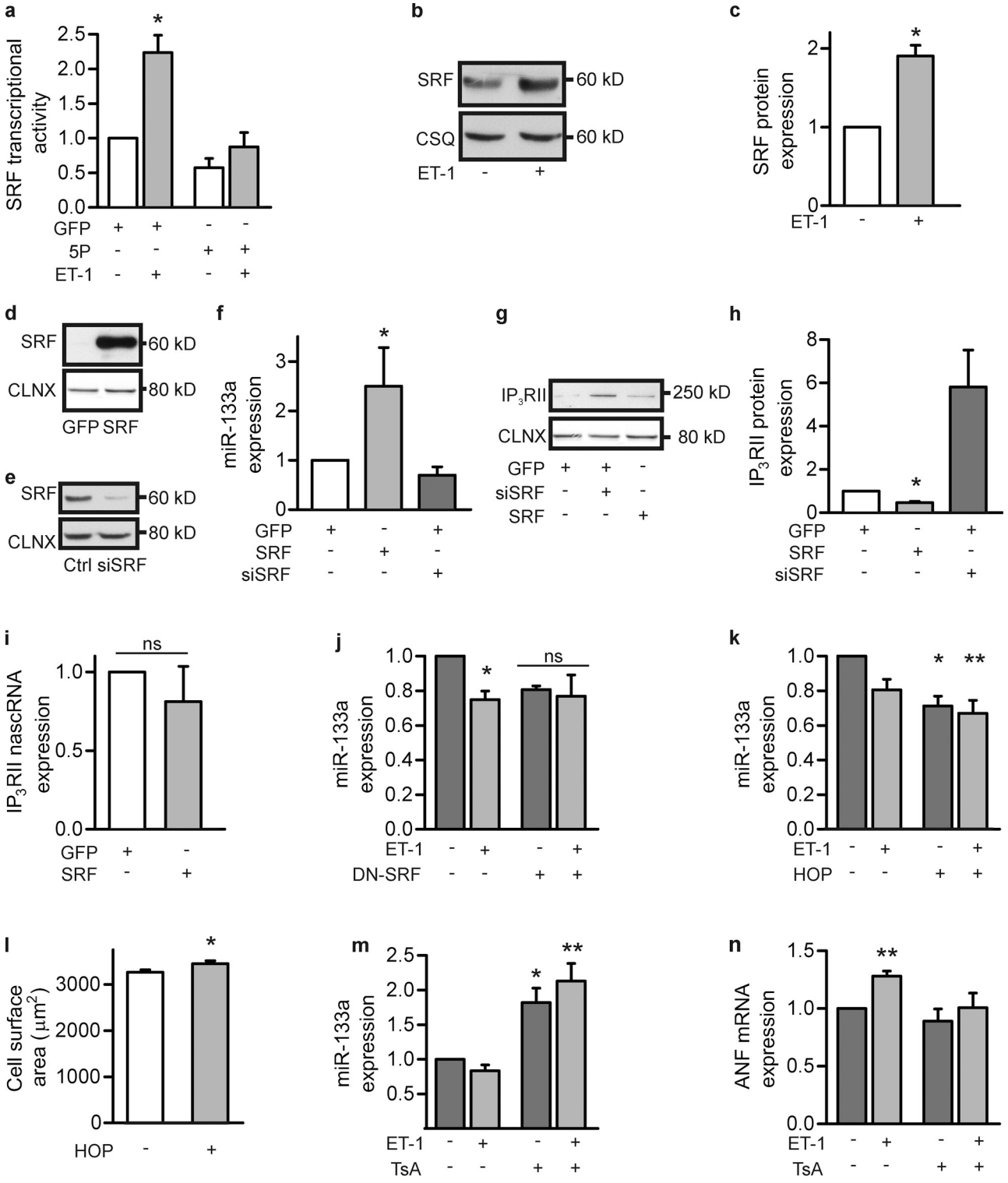

Figure 7. **IICR affects miR-133a expression through modulation of SRF activity.** (a) Luciferase reporter assay of SRF transcriptional activity in GFP/GFP-5P overexpressing NRVMs cultured in the presence and absence of 100 nM ET-1 for 24 h. (b) Immunoblot for SRF in control and ET-1–treated NRVM lysates. (c) Quantification of immunoblots as in b; $n = 6$. (d) Immunoblot for SRF in control or SRF-overexpressing NRVMs. (e) Immunoblot for SRF in control or siSRF-transfected NRVMs. (f) qPCR analysis of miR-133a expression in GFP control, SRF overexpressing, or SRF knockdown NRVMs. (g) Immunoblot to show IP_3RII expression in GFP-control, SRF-overexpressing, and SRF knockdown NRVMs. (h) Quantification of immunoblots as in g; $n = 4$. (i) IP_3RII nascent RNA expression in SRF-overexpressing NRVMs measured using qPCR. (j) qPCR analysis of miR-133a expression in control and DN-SRF–overexpressing NRVMs treated with ET-1. (k) miR-133a expression in control or HOP-overexpressing NRVMs cultured in the presence and absence of 100 nM ET-1 for 24 h. (l) Cell surface area quantification in control/HOP-overexpressing NRVMs. More than 300 cells taken from 4 separate experiments were measured per condition. (m) qPCR analysis of miR-133a expression in NRVMs treated with ET-1 in the presence and absence of 0.4 μM trichostatin A (TsA). (n) qPCR analysis of ANF expression in NRVMs treated as in k. Data are mean ± SEM from at least three independent experiments.*, $P < 0.05$; **, $P < 0.01$.

Published November 19, 2012

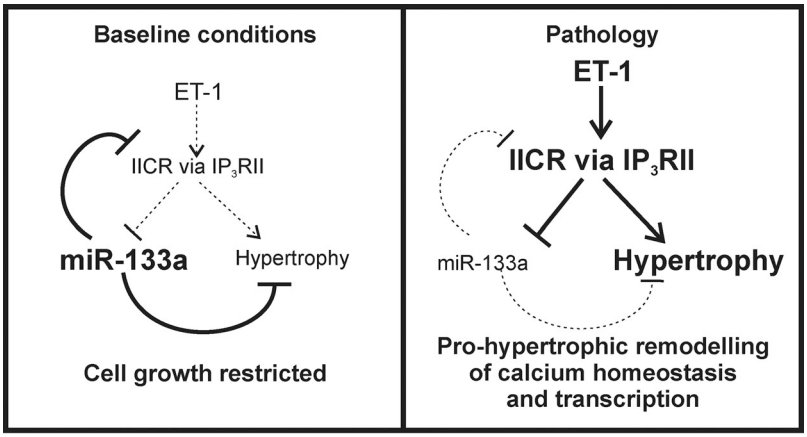

Figure 8. **IICR engages a pro-hypertrophic positive feedback loop.** Schematic diagram to represent how loss of miR-133a–mediated IP_3RII repression generates a positive feedback loop to drive the hypertrophic response.

The IICR-dependent transcriptional mechanism of origin for disease-associated repression of miR-133a is a significant finding. The murine genome encodes two copies of miR-133a: miR-133a-1 and miR-133a-2. These are located in the mouse in the vicinity of and cotranscribed with the sequences for miR1-2 and miR-1-1, respectively (Liu et al., 2007). Muscle-specific expression of the miR-133a, miR-1 bicistron is regulated by SRF and MEF2 (Zhao et al., 2005; Liu et al., 2007). Therefore, it is intriguing that miR-133a and miR-1 are repressed during hypertrophy, when global SRF activity is enhanced. However, different context-dependent modes of operation of SRF have been reported in other cellular systems, allowing a variable pattern of gene expression to be elicited without a change in bulk SRF activity (Wang et al., 2004). This is achieved through the association of SRF with diverse function-specific cofactors (Niu et al., 2007) including HOP, Nkx2.5, GATA4, Elk1, and myocardin. Regulation of these cofactors by intracellular signaling pathways allows positive or negative regulation of SRF in response to cellular stimulation. As calcium regulates multiple signal transducers including CaMKII, Cn-NFAT, and protein kinase C, there are a number of plausible mechanisms whereby the activity of SRF could be altered in response to IICR, preventing transcriptional activity at the miR-133a loci. We show that hypertrophy-associated decreases in miR-133a require HDAC activity and that overexpression of a dominant-negative SRF mutant or the negative transcriptional regulator HOP mimics the effect of ET-1 stimulation. This suggests that repression of SRF activity at the miR-133a loci may be a driving mechanism for the hypertrophy-associated decrease in miR-133a. Future work will aim to establish how IICR mediates decreased miR-133a expression via SRF, without similarly repressing expression of miR-1. The presence of additional transcription factor response elements between the miR-1 and miR-133a genes provides the potential for mechanisms of differential regulation (Thum et al., 2008).

Our data are consistent with previously published observations, which demonstrated that manipulation of miR-133a activity in vivo is sufficient to mediate pathological cardiac growth. In particular, infusion of miR-133a antagomir is sufficient to induce hypertrophic remodeling in adult mice (Carè et al., 2007). We have demonstrated that under these conditions, IP_3RII expression is increased, thus amplifying pro-hypertrophic IICR. miR-133a antagomir transfection generated a similar effect on myocyte phenotype eliciting both an increase in IP_3RII expression and hypertrophy. Notably, under these conditions we showed that IICR was required for the hypertrophic remodeling that arises as a consequence of a reduction in miR-133a activity. These data therefore show that as well as suppressing miR-133a abundance, IICR is the direct and required downstream mediator of hypertrophy induced by reduced miR-133a and further emphasizes the importance of miR-133a–mediated inhibition of IP_3RII for the restriction of pathological cellular growth. However, other studies have indicated that miR-133a maintains cardiac function via anti-apoptotic and anti-fibrotic effects within the adult myocardium (Matkovich et al., 2010). Some of the differences in the published data can be accounted for by variation in experimental model, the developmental stage from which miR-133a is expressed, the time-point at which observations are taken, and the extent to which adaptive mechanisms may be engaged in transgenic animals. Nevertheless, given the multitude of targets of any one miRNA and the complexity of regulation of myocyte gene expression networks, it is conceivable that more than one function exists for miR-133a in the maintenance of the healthy adult heart. Furthermore, the gross effect of a lack of miR-133a activity may change depending on the extent of disease progression, with different functions taking center stage over time. We believe that our data, by defining both a cause and consequence of dysregulated miR-133a centered on the IP_3RII, provide a new insight into how remodeling of calcium signaling and transcription promotes arrhythmias, left-ventricular hypertrophy, and eventually, heart failure.

Materials and methods

Animal procedures

All experiments involving animals were performed in accordance with local ethical and welfare guidelines. Specifically, for experiments in the UK, in accordance with the guidelines from the code of practice for humane killing under Schedule 1 of the Animals (Scientific Procedures) Act 1986 (UK); for experiments in Norway, The Guide for the Care and Use of Laboratory Animals published by the US National Institutes of Health (NIH publication no. 85–23, revised 1996); for experiments in the USA, The Institutional Animal Care and Use Committee (Cincinnati, OH); and for experiments in Japan, the Japanese Physiological Society.

Antibodies and other reagents

Antiserum against the IP_3RII C-terminal region (NH_2-CLGSNTPHVHHMPPH-OH) was raised in rat (Harzheim et al., 2009) and used for immunoblotting (IB) at

Published November 19, 2012

1:400 dilution and immunofluorescence (IF) at 1:50 dilution. Other antibodies were: RyR2 (IF 1:50; a gift from V. Sorrentino, University of Siena, Siena, Italy), calsequestrin (IB 1:15,000; PA1-913, Affinity Bioreagents), calnexin (IB 1:20,000; C4731, Sigma-Aldrich), α-actinin (IF 1:500; A7732; Sigma-Aldrich), and ANF (IF 1:500; T-4014, Bachem). Endothelin-1 was purchased from EMD Millipore. siRNA (Stealth) were from Invitrogen, miR-133a antagomirs were from GenePharma Ltd. Negative control target protector and custom target protectors C1, C2, and IP_3RII were designed by and purchased from QIAGEN. Adenovirus to express SRF was from T. Lee (Suny at Buffalo, Buffalo, NY). Unless stated otherwise, all other chemicals were purchased from Sigma-Aldrich.

HEK293 cell culture

HEK293 cells (Microbix) were cultured using standard tissue culture methods and maintained in DMEM medium containing 10% FBS and 1% penicillin/streptomycin/L-glutamine.

Preparation of neonatal rat ventricular myocytes

Cell isolation was essentially performed as described elsewhere (Higazi et al., 2009). In summary, Wistar rats (P3, Charles River Laboratories) were sacrificed by cervical dislocation and ventricles of beating hearts excised and placed in ice-cold neonatal myocyte buffer (20 mM Hepes, 100 mM NaCl, 5.4 mM KCl, 0.8 mM $MgSO_4$. 0.1% D-glucose, and 0.8 mM $NaH_2PO_4.H_2O$, pH 7.35). After washing to remove excess blood, hearts were minced into 2-mm^3 pieces using scissors and placed in 37°C digestion buffer (neonatal myocyte buffer containing 126 U/ml collagenase type II [Worthington], 0.2 mg/ml pancreatin, and 0.015 mg/ml DNase I [Roche]). Tissue was digested at 30°C with shaking at 190 rpm. 6 × 20-min digests were performed, and at the end of each incubation the tissue was triturated and the supernatant placed in myocyte plating medium (DMEM/M199 4:1 [Invitrogen], 10% donor horse serum [Invitrogen], 5% fetal calf serum [Invitrogen], 1 mM sodium pyruvate [PAA], 1× MEM nonessential amino acids [Invitrogen], 1× antibiotic-antimycotic [Invitrogen], and 3 µM cytosine β-D-arabinofuranoside). After every second digest, plating medium plus digested supernatant was passed through a 100-µm cell strainer and isolated cells collected by centrifugation (5 min, 390 *g*, room temperature). At the end of the digests, resuspended cells were preplated in a T175 flask and incubated for 45 min at 37°C to allow contaminating fibroblasts to adhere. Subsequently, myocytes were recovered by centrifugation (5 min, 390 *g*, room temperature). Cells were plated onto tissue culture vessels coated with 1% gelatin. Cultures were >95% pure. 48 h after plating, myocytes were washed into serum-free medium (DMEM/M199 4:1, 1 mM sodium pyruvate, 5.5 µg/ml transferrin, 5 ng/ml sodium selenite, 1× antibiotic-antimycotic, and 3 µM cytosine β-D-arabinofuranoside). Adenoviral infections were performed by incubation with a volume of virus-containing serum-free medium sufficient to cover the cells for 4 h. Agonist treatments diluted in serum-free medium were applied 24 h after infection with adenovirus.

Isolation and culture of ARVMs

Male SHR and WKY rats (Harlan) were anaesthetized by CO_2 inhalation and killed by cervical dislocation. After the thorax was opened, the heart was cannulated via the aorta and mounted on a modified Langendorff apparatus. All buffers were warmed to 37°C and oxygenated before use. Hepes buffer (10 mM Hepes, 135 mM NaCl, 5.4 mM KCl, 10 mM D-glucose, 2 mM $MgCl_2$, and 1 mM $CaCl_2$, pH 7.35) was perfused in a retrograde manner for 4 min after which a low calcium buffer (10 mM Hepes, 120 mM NaCl, 5.4 mM KCl, 20 mM taurine, 20 mM D-glucose, 5 mM $MgSO_4$, 5 mM sodium pyruvate, 5.5 mM NTA, and 80 µM $CaCl_2$, pH 6.98) was perfused for 3.5 min. Enzyme buffer (10 mM Hepes, 120 mM NaCl, 5.4 mM KCl, 20 mM taurine, 20 mM D-glucose, 5 mM $MgSO_4$, 5 mM sodium pyruvate, 35 µM $CaCl_2$, and 319 U/ml collagenase type II [Worthington], pH 7.4) was circulated for 9.5 min. The heart was then removed from the apparatus and cut into ~3-mm^3 chunks. 30 ml enzyme solution was added and an incubation performed for 4.5 min with shaking at 300 oscillations/min. Enzyme solution was replaced and a second 4.5-min incubation performed. The supernatant was then replaced with enzyme solution lacking collagenase and the tissue triturated to release cells. Supernatant containing cells was transferred to a fresh tube and the cells allowed to sediment under gravity. The resulting pellet was resuspended in adult myocyte medium (M199, 1% penicillin/streptomycin/L-glutamine, and 0.2% BSA) and the cells plated onto laminin-coated (25 µg/ml; Invitrogen) dishes. Cells were allowed to adhere for 1 h before replacement of medium. Adenoviral infections were performed overnight in a minimal volume of virus-containing medium.

Adult rat thoracic aortic constriction and echocardiography

~170-g male Wistar rats were anesthetized by a mixture of 67% N_2O, 27% O_2, and 4% isoflurane, and subsequently intubated and ventilated with a mixture of 67% N_2O, 28% O_2, and 2% isoflurane. The ascending aorta was dissected through a right-sided thoracotomy, and a silk suture (3–0) was tightened around the ascending aorta and a steel wire (0.85 mm) proximal to the brachiocephalic trunk as described previously (Brattelid et al., 2007). Immediately after the ligation, the steel wire was removed. The chest was closed and the rats extubated. Sham-operated animals served as controls and underwent the same surgical procedure, except tightening the silk suture around the ascending aorta. Buprenorphine was given as postoperative analgesia.

6 wks after aortic banding, rats were anesthetized by a mixture of 66% N_2O, 27% O_2, and 4% isoflurane, and subsequently mask ventilated with a mixture of 67% N_2O, 28% O_2, and 2% isoflurane. Vevo 2100 (VisualSonics) with a 24-MHz Microscan linear phased array transducer was used to obtain echocardiographic examinations. Ventricular dimensions and Doppler signals were recorded in the parasternal long axis view. After echocardiography, rats were intubated and ventilated through endotracheal intubation. The chest was opened, followed by excision of the heart. The four heart chambers were rapidly dissected, weighed, and frozen in liquid nitrogen. Left ventricular myocardium was used for further molecular analysis.

Mouse models

Protocols for generation of IP_3RII and IP_3-sponge transgenic mice and TAC of modified mice have been described previously (Nakayama et al., 2006, 2010). Cardiac-specific expression of mouse IP_3RII or flag-tagged IP_3-sponge protein was generated by placing the respective cDNAs under the control of the inducible α-myosin heavy chain promoter (Sanbe et al., 2003). Transgenic mice overexpressing these proteins were crossed with driver tetracycline transactivator transgenic mice. IP_3RII knockout mice are disrupted within the first coding exon of the *Itpr2* gene (Futatsugi et al., 2005). Single-transgenic miR133a-$1^{neo/+}$ or miR133a-$2^{neo/+}$ knockout mice were generated by replacing 68 bp of the premiR133a-1 stem-loop or 108 bp of the premiR133a-2 stem-loop with a neomycin resistance cassette flanked by 2 FRT sites (Liu et al., 2008). Double heterozygote mice were generated by crossing miR133a-$1^{neo/+}$ with miR133a-$2^{neo/+}$ mice and then intercrossed to obtain double knockout mice lacking both miR133a-1 and miR133a-2.

Methods for infusion of mice with saline or the antagomir oligo via osmotic mini-pump are described in Carè et al. (2007). In brief, antagomirs were dissolved in saline solution at doses of 80 mg/kg body weight and loaded in Alzet osmotic minipumps (model 1003D; Alza). To prime the pumps for continuous delivery of the antagomir, loaded minipumps were placed in a flask with saline solution and incubated for 4 h at 37°C. Activated minipumps were then implanted subcutaneously.

Molecular biology and preparation of adenovirus

To construct the *Itpr2* 3′UTR luciferase reporter, the *Itpr2* 3′UTR was PCR amplified from rat liver genomic DNA and cloned into psiChk2 (Promega). Due to the presence of an internal XhoI site within the *Itpr2* 3′UTR, PCR amplification and subcloning was performed in two stages. First, the 3′UTR was PCR amplified, digested with XhoI and NotI, and inserted into psiChk2. Forward primer sequence: 5′-CACCGCTCGAGCACCATGGGGGCACGCCGTGAC-3′, reverse primer sequence: 5′-CAGTGGCGGCCGCCTAATTACAAACAATTATTTTAAT-3′. This inserted the 3′ section of the 3′UTR into psiChk2. Next, the 5′ end of the 3′UTR was PCR amplified, digested with XhoI, and inserted into the XhoI site of psiChk2 to recreate the full-length *Itpr2* 3′UTR. Forward primer sequence: 5′-CACCGCTCGAGCACCATGGGGGCACGCCGTGAC-3′, reverse primer sequence: 5-GTTGGCTGTTACCCTCGAGTTT-3′. The resulting product was sequenced to ensure fidelity with the genomic sequence. To mutate the miR-133a binding site within the *Itpr2* 3′UTR, QuikChange site-directed mutagenesis (Stratagene) was performed at eight positions, according to the manufacturer's instructions.

The miR-133a precursor transcript was PCR amplified from rat liver genomic DNA and cloned into psi-RNA-h7SK-GFP (Invivogen) using the Acc651 and HindIII sites. Forward primer sequence: 5′-CCTAGGTACCAGACTCTACACTAGTGTGGGACCCTC-3′, reverse primer sequence: 5′-CATAAAGCTTTCAAGAAACATC-3′. To allow generation of adenovirus, miR-133a was PCR amplified from psi-RNA-h7SK-GFP miR-133a and inserted into the MluI and HindIII sites of pRNAT H1.2 Adeno (Genscript). Forward primer sequence: 5′-GGTACCACGCGTACACTAGTGTGGGACCCTC-3′, reverse primer sequence: 5′-CATAAAGCTTTCAAGAAACATC-3′. A nonfluorescent adenoviral shuttle vector (pShuttle H1 miR-133a) was created by subcloning the H1 promoter and miR-133a from pRNAT H1.2 miR-133a into pShuttle using the BglII and HindIII sites. C-myc–tagged HOP sequence was excised from pcDNA3.1 HOP (a gift from J.A. Epstein,

Published November 19, 2012

University of Pennsylvania, Philadelphia, PA) using PmeI and inserted into EcoRV-digested pShuttle-CMV. Recombinant adenoviral constructs were produced from pRNAT H1.2 miR-133a GFP, pShuttle H1 miR-133a, and pShuttle CMV HOP using the AdEasy method (Luo et al., 2007). PacI-digested recombinant plasmids were transfected into HEK293 cells and crude adenovirus harvested after 10–14 d. This crude viral preparation was used for large-scale amplification of virus in HEK293 cells, which was purified using the Vivapure Adenopack 100 (Sartorius).

Gene expression analysis

Total RNA was isolated from cardiac myocytes and tissue samples using the miRVana-miRNA isolation kit (Ambion) and cDNA was synthesized from 500 ng total RNA using the NCode Vilo miRNA cDNA synthesis kit (Invitrogen). qPCR was performed using SYBR-GreenER (Invitrogen) and primers specific for the sequence of interest. Reactions were performed using a Real-Time PCR Cycler (model CFX96; Bio-Rad Laboratories). For the analysis of mRNA expression, primers amplified targets spanning exon–exon boundaries. To analyze nascent RNA, expression primers amplified targets within the intron, allowing unspliced IP_3RII RNA to be quantified. GAPDH, β_2-microglobulin, and troponin T were used as internal normalization controls. Analysis was performed using the comparative ΔC_t method (Vandesompele et al., 2002), whereby the geometric mean of the expression levels of three independent normalization controls is calculated and used as a normalization factor to compare the expression level of the gene of interest between samples from different experimental conditions.

Protein expression analysis

Tissue samples were placed in lysis buffer (10 mM Tris-HCl, pH 7.6, 1 mM DTT, 1 mM EGTA, and protease and phosphatase inhibitor cocktails [Sigma-Aldrich]) and homogenized in a lysing matrix D tube (MP Bio) for 30 s at 40 m/s in a FastPrep machine (MPBio). Debris was pelleted by centrifugation for 1 min at 3,500 *g* and the remaining supernatant incubated on ice for 30 min. Cultured cells were harvested by scraping in PBS, recovered by centrifugation, resuspended in lysis buffer, and incubated on ice for 30 min. The membrane fraction was recovered from all sample types by centrifuging the lysate for 15 min at 100,000 *g* (4°C), and the resulting pellet solubilized in lysis buffer containing 140 mM NaCl and 1% Triton X-100. Protein concentration was determined using the BCA assay (Thermo Fisher Scientific) and equivalent amounts of protein were resolved on 7% SDS polyacrylamide gels. Proteins were transferred to PVDF membranes and analyzed by immunoblotting with appropriate primary antibodies and HRP-conjugated secondary antibodies. Immunoreactive bands were detected by enhanced chemiluminescence (Thermo Fisher Scientific).

Transfections

HEK293 cells cultured in 48-well dishes were transfected with the *Itpr2* 3′UTR reporter/mutant 3′UTR reporter and psi-RNA-h7SK-GFP miR-133a using Lipofectamine 2000 (Invitrogen) according to the manufacturer's instructions. Lipofectamine 2000 was also used for transfection of NRVMs with the *Itpr2* 3′UTR reporter, antagomir oligos, and siRNA. For target protector (TP; QIAGEN) transfection of NRVMs, Dharmafect I and Accell medium (Dharmacon) were used according to the manufacturer's protocol. TPs were: manufacturer's negative control without homology to any known mammalian gene, *Itpr2* miR-133a-site specific TP, TP C1, which binds 89 base pairs downstream of the miR-133a site, and TP C2, which binds 306 base pairs downstream of the miR-133a site. C1 and C2 were designed to bind to sites proximal to, but not overlapping with the miR-133a site and within regions of the *Itpr2* 3′-UTR without binding sites for known hypertrophy-associated miRNAs.

Luciferase reporter assay

NRVMs or HEK293 cultured in 48-well dishes were lysed using 1× passive lysis buffer (Promega). Luciferase reporter assays were performed using 10 µl lysate and the dual reporter luciferase assay kit (Promega), according to the manufacturer's protocol.

Immunofluorescence analysis

For analysis of cell surface area, NRVMs were cultured in Falcon black 96-well imaging plates (BD) coated with 1% gelatin. At the end of the experiment, cells were washed in PBS and fixed by incubation in PBS containing 2% paraformaldehyde/0.05% glutaraldehyde for 15 min at room temperature. Immunofluorescent staining of cells for α-actinin and ANF was performed as in Higazi et al. (2009). Alexa Fluor 488– and 568–coupled secondary antibodies (Invitrogen) were used at 1:500 dilution. At the end of the staining protocol, nuclei were stained by incubation for 20 min at room temperature with Hoescht (1 µg/ml in PBS; Invitrogen). Images were captured at room temperature using the Pathway 855 high-content imaging system (BD) and AttoVision software (BD). The microscope was equipped with a 40× (0.75 NA) UPlan FLN air objective (Olympus) and an Orca ER camera (Hamamatsu Photonics). For surface area measurements, images were analyzed by drawing around the edge of the cells in ImageJ (National Institutes of Health). At least 400 cells from 3 independent experiments were analyzed. These images were also used to quantify ANF protein expression by counting the number of NRVMs exhibiting a perinuclear ring of ANF.

For analysis of IP_3RII and RyR2 expression in isolated ventricular myocytes from sham and AB rats, myocytes were permeabilized for 15 min in 0.2% Triton X-100/PBS. Nonspecific antibody binding was blocked by incubation in blocking buffer (5% chemiblocker [EMD Millipore] in 0.1% Triton X-100/PBS) for 1 h at 4°C. Primary antibodies were diluted in blocking buffer and incubations performed overnight at 4°C. Alexa Fluor 488– and 647–coupled secondary antibodies were diluted 1:500 in blocking buffer and incubated for 1 h at 4°C. Samples were mounted onto slides using Vectashield with DAPI (Vector Laboratories). Confocal imaging was performed at room temperature using a microscope (model A1R; Nikon) and a violet-corrected 60× oil immersion objective (1.4 NA). Cells were imaged at a zoom of 1.79, which allowed for a whole cell to be imaged in the image field. Dimensions were in the order of 0.11 µm/pixel and z-sections were taken at 0.15-µm intervals through a 5-µm volume around the mid-nuclear plain. Stacks were deconvolved using AutoQuant software (setting high noise, with 10 iterations). For 2D Fourier analysis (FFT), the mid-nuclear section of these stacks was rotated so that the z-line striations were located horizontally in the field (using ImageJ) and an area of 200 × 200 pixels was cropped. Care was taken for the cropped image to contain both the perinuclear and the junctional regions of the myocyte. These images were then submitted to 2D Fourier analysis (ImageJ).

Confocal calcium imaging

WKY myocytes cultured on laminin-coated 16-mm coverslips were infected overnight with adenovirus to overexpress miR-133a or with empty vector control virus (both without fluorescent protein expression). The next morning, culture medium was removed and cells were loaded with 8 µM fluo-4 (Invitrogen) in Hepes buffer for 30 min at room temperature. After this incubation and one wash in Hepes buffer, cells were incubated in Hepes buffer for a further 30 min to de-esterify the dye. Coverslips were then placed in a pacing chamber on the stage of a confocal imaging system (A1R; Nikon) and electrically paced at 0.33 Hz, 30 V at room temperature throughout the experiment. Only rod-shaped cells showing regular calcium transients in response to pacing were selected for further analysis. Movies were captured in NIS elements software at 120 frames/s with averaging every 2 frames, section thickness = 1.52 µm, using a 60× (1.40 NA) Apo violet-corrected oil objective (Nikon) and 488-nm laser to excite fluo-4 fluorescence. Imaging was performed for 20 s every 30 s with the addition of 1 mM tetracaine in Hepes buffer and 1 mM tetracaine + 10 µM IP_3 ester (a gift from S. Conway, University of Oxford, Oxford, UK) at the start of the second and third movies, respectively. A total of six movies was captured per cell. ImageJ was used to background subtract the data. Calcium release events were detected using SparkSpotter, an ImageJ plugin developed by Babraham Bioinformatics, which counted events with at least 100 intensity units difference above the mean value that lasted at least 4 frames.

Statistical analysis

Results are presented as mean ± SEM. Statistical analyses were performed in GraphPad Prism using the one-sample *t* test for two groups and one-way Anova followed by Tukey analysis for two or more groups. P values <0.05 were considered significant.

Online supplemental material

Fig. S1 (a and b) shows 2D Fourier analysis of IP_3RII and RyR2 expression in ventricular myocytes from sham and AB rats. Fig. S1 c shows qPCR quantification of miR-133a expression in cardiomyocytes and noncardiomyocytes. Fig. S2 shows IP_3RII expression in NRVMs transfected with control TPs or specific IP_3RII TP. Fig. S3 a shows qPCR quantification of miR-133a expression levels in ARVMs expressing GFP/GFP-miR-133a. Fig. S3 b shows IP_3RII protein expression in ARVMs expressing GFP/GFP-miR-133a. Fig. S4 a is an immunoblot showing IP_3RII expression in control mice and mice infused with scrambled miR-133a antagomir. Fig. S4 b is quantification of blots as in Fig. S4 a. Fig. S5 a is qPCR quantification of miR-1 expression in control and IP_3RII-transgenic mice. Fig. S5 b shows miR-1 expression in control mice and mice overexpressing the IP_3-sponge

protein. Fig. S5 c shows qPCR quantification of miR-1 expression in wild-type and IP_3RII knockout mice. Online supplemental material is available at http://www.jcb.org/cgi/content/full/jcb.201111095/DC1.

We are grateful to S. Conway for IP_3 ester; T. Lee for the SRF adenovirus; J.A. Epstein for HOP plasmids; V. Sorrentino for the RyR2 antibody; S. Walker and C. Seal (Imaging Facility, Babraham Institute, Cambridge, UK) for assistance with imaging; and the Roderick and Bootman laboratories for assistance throughout this work.

This work was supported by the British Heart Foundation (PG/07/040, PG/06/034), The Babraham Institute, The Royal Society (University Research Fellowship to H.L. Roderick), and the Biotechnology and Biological Sciences Research Council.

Submitted: 21 November 2011
Accepted: 25 October 2012

References

Bartel, D.P. 2004. MicroRNAs: genomics, biogenesis, mechanism, and function. *Cell*. 116:281–297. http://dx.doi.org/10.1016/S0092-8674(04)00045-5

Bartel, D.P., and C.Z. Chen. 2004. Micromanagers of gene expression: the potentially widespread influence of metazoan microRNAs. *Nat. Rev. Genet.* 5:396–400. http://dx.doi.org/10.1038/nrg1328

Belaguli, N.S., W. Zhou, T.H. Trinh, M.W. Majesky, and R.J. Schwartz. 1999. Dominant negative murine serum response factor: alternative splicing within the activation domain inhibits transactivation of serum response factor binding targets. *Mol. Cell. Biol.* 19:4582–4591.

Berridge, M.J., M.D. Bootman, and H.L. Roderick. 2003. Calcium signalling: dynamics, homeostasis and remodelling. *Nat. Rev. Mol. Cell Biol.* 4:517–529. http://dx.doi.org/10.1038/nrm1155

Brattelid, T., E. Qvigstad, J.A. Birkeland, F. Swift, S.V. Bekkevold, K.A. Krobert, O.M. Sejersted, T. Skomedal, J.B. Osnes, F.O. Levy, and I. Sjaastad. 2007. Serotonin responsiveness through 5-HT2A and 5-HT4 receptors is differentially regulated in hypertrophic and failing rat cardiac ventricle. *J. Mol. Cell. Cardiol.* 43:767–779. http://dx.doi.org/10.1016/j.yjmcc.2007.08.019

Cao, D.J., Z.V. Wang, P.K. Battiprolu, N. Jiang, C.R. Morales, Y. Kong, B.A. Rothermel, T.G. Gillette, and J.A. Hill. 2011. Histone deacetylase (HDAC) inhibitors attenuate cardiac hypertrophy by suppressing autophagy. *Proc. Natl. Acad. Sci. USA*. 108:4123–4128. http://dx.doi.org/10.1073/pnas.1015081108

Carè, A., D. Catalucci, F. Felicetti, D. Bonci, A. Addario, P. Gallo, M.L. Bang, P. Segnalini, Y. Gu, N.D. Dalton, et al. 2007. MicroRNA-133 controls cardiac hypertrophy. *Nat. Med.* 13:613–618. http://dx.doi.org/10.1038/nm1582

Choi, W.-Y., A.J. Giraldez, and A.F. Schier. 2007. Target protectors reveal dampening and balancing of Nodal agonist and antagonist by miR-430. *Science*. 318:271–274. http://dx.doi.org/10.1126/science.1147535

da Costa Martins, P.A., K. Salic, M.M. Gladka, A.-S. Armand, S. Leptidis, H. el Azzouzi, A. Hansen, C.J. Coenen-de Roo, M.F. Bierhuizen, R. van der Nagel, et al. 2010. MicroRNA-199b targets the nuclear kinase Dyrk1a in an auto-amplification loop promoting calcineurin/NFAT signalling. *Nat. Cell Biol.* 12:1220–1227. http://dx.doi.org/10.1038/ncb2126

Dillmann, W.H. 2008. The rat as a model for cardiovascular disease. *Drug Discov. Today Dis. Models*. 5:173–178. http://dx.doi.org/10.1016/j.ddmod.2009.03.006

Dong, D.L., C. Chen, R. Huo, N. Wang, Z. Li, Y.J. Tu, J.T. Hu, X. Chu, W. Huang, and B.F. Yang. 2010. Reciprocal repression between microRNA-133 and calcineurin regulates cardiac hypertrophy: a novel mechanism for progressive cardiac hypertrophy. *Hypertension*. 55:946–952. http://dx.doi.org/10.1161/HYPERTENSIONAHA.109.139519

Dorn, G.W. II. 2007. The fuzzy logic of physiological cardiac hypertrophy. *Hypertension*. 49:962–970. http://dx.doi.org/10.1161/HYPERTENSIONAHA.106.079426

Drawnel, F.M., C.R. Archer, and H.L. Roderick. 2012. The role of the paracrine/autocrine mediator endothelin-1 in regulation of cardiac contractility and growth. *Br. J. Pharmacol.*

Elia, L., R. Contu, M. Quintavalle, F. Varrone, C. Chimenti, M.A. Russo, V. Cimino, L. De Marinis, A. Frustaci, D. Catalucci, and G. Condorelli. 2009. Reciprocal regulation of microRNA-1 and insulin-like growth factor-1 signal transduction cascade in cardiac and skeletal muscle in physiological and pathological conditions. *Circulation*. 120:2377–2385. http://dx.doi.org/10.1161/CIRCULATIONAHA.109.879429

Futatsugi, A., T. Nakamura, M.K. Yamada, E. Ebisui, K. Nakamura, K. Uchida, T. Kitaguchi, H. Takahashi-Iwanaga, T. Noda, J. Aruga, and K. Mikoshiba. 2005. IP3 receptor types 2 and 3 mediate exocrine secretion underlying energy metabolism. *Science*. 309:2232–2234. http://dx.doi.org/10.1126/science.1114110

Guatimosim, S., M.J. Amaya, M.T. Guerra, C.J. Aguiar, A.M. Goes, N.L. Gómez-Viquez, M.A. Rodrigues, D.A. Gomes, J. Martins-Cruz, W.J. Lederer, and M.F. Leite. 2008. Nuclear Ca2+ regulates cardiomyocyte function. *Cell Calcium*. 44:230–242. http://dx.doi.org/10.1016/j.ceca.2007.11.016

Guo, A., S.E. Cala, and L.S. Song. 2012. Calsequestrin accumulation in rough endoplasmic reticulum promotes perinuclear Ca2+ release. *J. Biol. Chem.* 287:16670–16680. http://dx.doi.org/10.1074/jbc.M112.340927

Haider, A.W., M.G. Larson, E.J. Benjamin, and D. Levy. 1998. Increased left ventricular mass and hypertrophy are associated with increased risk for sudden death. *J. Am. Coll. Cardiol.* 32:1454–1459. http://dx.doi.org/10.1016/S0735-1097(98)00407-0

Harzheim, D., M. Movassagh, R.S. Foo, O. Ritter, A. Tashfeen, S.J. Conway, M.D. Bootman, and H.L. Roderick. 2009. Increased InsP3Rs in the junctional sarcoplasmic reticulum augment Ca2+ transients and arrhythmias associated with cardiac hypertrophy. *Proc. Natl. Acad. Sci. USA*. 106:11406–11411. http://dx.doi.org/10.1073/pnas.0905485106

Harzheim, D., A. Talasila, M. Movassagh, R.S. Foo, N. Figg, M.D. Bootman, and H.L. Roderick. 2010. Elevated InsP3R expression underlies enhanced calcium fluxes and spontaneous extra-systolic calcium release events in hypertrophic cardiac myocytes. *Channels (Austin)*. 4:67–71. http://dx.doi.org/10.4161/chan.4.1.10531

Higazi, D.R., C.J. Fearnley, F.M. Drawnel, A. Talasila, E.M. Corps, O. Ritter, F. McDonald, K. Mikoshiba, M.D. Bootman, and H.L. Roderick. 2009. Endothelin-1-stimulated InsP3-induced Ca2+ release is a nexus for hypertrophic signaling in cardiac myocytes. *Mol. Cell*. 33:472–482. http://dx.doi.org/10.1016/j.molcel.2009.02.005

Hill, J.A., M. Karimi, W. Kutschke, R.L. Davisson, K. Zimmerman, Z. Wang, R.E. Kerber, and R.M. Weiss. 2000. Cardiac hypertrophy is not a required compensatory response to short-term pressure overload. *Circulation*. 101:2863–2869. http://dx.doi.org/10.1161/01.CIR.101.24.2863

Ikeda, S., S.W. Kong, J. Lu, E. Bisping, H. Zhang, P.D. Allen, T.R. Golub, B. Pieske, and W.T. Pu. 2007. Altered microRNA expression in human heart disease. *Physiol. Genomics*. 31:367–373. http://dx.doi.org/10.1152/physiolgenomics.00144.2007

Kjeldsen, S.E., B. Dahlöf, R.B. Devereux, S. Julius, P. Aurup, J. Edelman, G. Beevers, U. de Faire, F. Fyhrquist, H. Ibsen, et al. 2002. Effects of losartan on cardiovascular morbidity and mortality in patients with isolated systolic hypertension and left ventricular hypertrophy: a Losartan Intervention for Endpoint Reduction (LIFE) substudy. *JAMA*. 288:1491–1498. http://dx.doi.org/10.1001/jama.288.12.1491

Kook, H., J.J. Lepore, A.D. Gitler, M.M. Lu, W. Wing-Man Yung, J. Mackay, R. Zhou, V. Ferrari, P. Gruber, and J.A. Epstein. 2003. Cardiac hypertrophy and histone deacetylase-dependent transcriptional repression mediated by the atypical homeodomain protein Hop. *J. Clin. Invest.* 112:863–871.

Li, Q., X. Lin, X. Yang, and J. Chang. 2010a. NFATc4 is negatively regulated in miR-133a-mediated cardiomyocyte hypertrophic repression. *Am. J. Physiol. Heart Circ. Physiol.* 298:H1340–H1347. http://dx.doi.org/10.1152/ajpheart.00592.2009

Li, Q., X.-W. Song, J. Zou, G.-K. Wang, E. Kremneva, X.-Q. Li, N. Zhu, T. Sun, P. Lappalainen, W.-J. Yuan, et al. 2010b. Attenuation of microRNA-1 derepresses the cytoskeleton regulatory protein twinfilin-1 to provoke cardiac hypertrophy. *J. Cell Sci.* 123:2444–2452. http://dx.doi.org/10.1242/jcs.067165

Lim, L.P., N.C. Lau, P. Garrett-Engele, A. Grimson, J.M. Schelter, J. Castle, D.P. Bartel, P.S. Linsley, and J.M. Johnson. 2005. Microarray analysis shows that some microRNAs downregulate large numbers of target mRNAs. *Nature*. 433:769–773. http://dx.doi.org/10.1038/nature03315

Lipp, P., M. Laine, S.C. Tovey, K.M. Burrell, M.J. Berridge, W. Li, and M.D. Bootman. 2000. Functional InsP3 receptors that may modulate excitation-contraction coupling in the heart. *Curr. Biol.* 10:939–942. http://dx.doi.org/10.1016/S0960-9822(00)00624-2

Liu, N., A.H. Williams, Y. Kim, J. McAnally, S. Bezprozvannaya, L.B. Sutherland, J.A. Richardson, R. Bassel-Duby, and E.N. Olson. 2007. An intragenic MEF2-dependent enhancer directs muscle-specific expression of microRNAs 1 and 133. *Proc. Natl. Acad. Sci. USA*. 104:20844–20849. http://dx.doi.org/10.1073/pnas.0710558105

Liu, N., S. Bezprozvannaya, A.H. Williams, X. Qi, J.A. Richardson, R. Bassel-Duby, and E.N. Olson. 2008. microRNA-133a regulates cardiomyocyte proliferation and suppresses smooth muscle gene expression in the heart. *Genes Dev.* 22:3242–3254. http://dx.doi.org/10.1101/gad.1738708

Luo, D., D. Yang, X. Lan, K. Li, X. Li, J. Chen, Y. Zhang, R.P. Xiao, Q. Han, and H. Cheng. 2008. Nuclear Ca2+ sparks and waves mediated by inositol 1,4,5-trisphosphate receptors in neonatal rat cardiomyocytes. *Cell Calcium*. 43:165–174. http://dx.doi.org/10.1016/j.ceca.2007.04.017

Luo, J., Z.L. Deng, X. Luo, N. Tang, W.X. Song, J. Chen, K.A. Sharff, H.H. Luu, R.C. Haydon, K.W. Kinzler, et al. 2007. A protocol for rapid generation of recombinant adenoviruses using the AdEasy system. *Nat. Protoc.* 2:1236–1247. http://dx.doi.org/10.1038/nprot.2007.135

Matkovich, S.J., W. Wang, Y. Tu, W.H. Eschenbacher, L.E. Dorn, G. Condorelli, A. Diwan, J.M. Nerbonne, and G.W. Dorn II. 2010. MicroRNA-133a protects against myocardial fibrosis and modulates electrical repolarization without affecting hypertrophy in pressure-overloaded adult hearts. *Circ. Res.* 106:166–175. http://dx.doi.org/10.1161/CIRCRESAHA.109.202176

Matkovich, S.J., D.J. Van Booven, W.H. Eschenbacher, and G.W. Dorn II. 2011. RISC RNA sequencing for context-specific identification of in vivo microRNA targets. *Circ. Res.* 108:18–26. http://dx.doi.org/10.1161/CIRCRESAHA.110.233528

Nakayama, H., B.J. Wilkin, I. Bodi, and J.D. Molkentin. 2006. Calcineurin-dependent cardiomyopathy is activated by TRPC in the adult mouse heart. *FASEB J.* 20:1660–1670. http://dx.doi.org/10.1096/fj.05-5560com

Nakayama, H., I. Bodi, M. Maillet, J. DeSantiago, T.L. Domeier, K. Mikoshiba, J.N. Lorenz, L.A. Blatter, D.M. Bers, and J.D. Molkentin. 2010. The IP3 receptor regulates cardiac hypertrophy in response to select stimuli. *Circ. Res.* 107:659–666. http://dx.doi.org/10.1161/CIRCRESAHA.110.220038

Niu, Z., A. Li, S.X. Zhang, and R.J. Schwartz. 2007. Serum response factor micromanaging cardiogenesis. *Curr. Opin. Cell Biol.* 19:618–627. http://dx.doi.org/10.1016/j.ceb.2007.09.013

Perez, P.J., J. Ramos-Franco, M. Fill, and G.A. Mignery. 1997. Identification and functional reconstitution of the type 2 inositol 1,4,5-trisphosphate receptor from ventricular cardiac myocytes. *J. Biol. Chem.* 272:23961–23969. http://dx.doi.org/10.1074/jbc.272.38.23961

Posern, G., and R. Treisman. 2006. Actin' together: serum response factor, its cofactors and the link to signal transduction. *Trends Cell Biol.* 16:588–596. http://dx.doi.org/10.1016/j.tcb.2006.09.008

Rinne, A., and L.A. Blatter. 2010. Activation of NFATc1 is directly mediated by IP3 in adult cardiac myocytes. *Am. J. Physiol. Heart Circ. Physiol.* 299:H1701–H1707. http://dx.doi.org/10.1152/ajpheart.00470.2010

Sanbe, A., J. Gulick, M.C. Hanks, Q. Liang, H. Osinska, and J. Robbins. 2003. Reengineering inducible cardiac-specific transgenesis with an attenuated myosin heavy chain promoter. *Circ. Res.* 92:609–616. http://dx.doi.org/10.1161/01.RES.0000065442.64694.9F

Sayed, D., C. Hong, I.-Y. Chen, J. Lypowy, and M. Abdellatif. 2007. MicroRNAs play an essential role in the development of cardiac hypertrophy. *Circ. Res.* 100:416–424. http://dx.doi.org/10.1161/01.RES.0000257913.42552.23

Small, E.M., and E.N. Olson. 2011. Pervasive roles of microRNAs in cardiovascular biology. *Nature*. 469:336–342. http://dx.doi.org/10.1038/nature09783

Thum, T., D. Catalucci, and J. Bauersachs. 2008. MicroRNAs: novel regulators in cardiac development and disease. *Cardiovasc. Res.* 79:562–570. http://dx.doi.org/10.1093/cvr/cvn137

Tovey, S.C., P. de Smet, P. Lipp, D. Thomas, K.W. Young, L. Missiaen, H. De Smedt, J.B. Parys, M.J. Berridge, J. Thuring, et al. 2001. Calcium puffs are generic InsP(3)-activated elementary calcium signals and are downregulated by prolonged hormonal stimulation to inhibit cellular calcium responses. *J. Cell Sci.* 114:3979–3989.

Uchiyama, T., F. Yoshikawa, A. Hishida, T. Furuichi, and K. Mikoshiba. 2002. A novel recombinant hyperaffinity inositol 1,4,5-trisphosphate (IP(3)) absorbent traps IP(3), resulting in specific inhibition of IP(3)-mediated calcium signaling. *J. Biol. Chem.* 277:8106–8113. http://dx.doi.org/10.1074/jbc.M108337200

van Rooij, E., L.B. Sutherland, N. Liu, A.H. Williams, J. McAnally, R.D. Gerard, J.A. Richardson, and E.N. Olson. 2006. A signature pattern of stress-responsive microRNAs that can evoke cardiac hypertrophy and heart failure. *Proc. Natl. Acad. Sci. USA*. 103:18255–18260. http://dx.doi.org/10.1073/pnas.0608791103

van Rooij, E., L.B. Sutherland, X. Qi, J.A. Richardson, J. Hill, and E.N. Olson. 2007. Control of stress-dependent cardiac growth and gene expression by a microRNA. *Science*. 316:575–579. http://dx.doi.org/10.1126/science.1139089

Vandesompele, J., K. De Preter, F. Pattyn, B. Poppe, N. Van Roy, A. De Paepe, and F. Speleman. 2002. Accurate normalization of real-time quantitative RT-PCR data by geometric averaging of multiple internal control genes. *Genome Biol.* 3:H0034–h0034.11. http://dx.doi.org/10.1186/gb-2002-3-7-research0034

Wang, Z., D.-Z. Wang, D. Hockemeyer, J. McAnally, A. Nordheim, and E.N. Olson. 2004. Myocardin and ternary complex factors compete for SRF to control smooth muscle gene expression. *Nature*. 428:185–189. http://dx.doi.org/10.1038/nature02382

Wu, X., T. Zhang, J. Bossuyt, X. Li, T.A. McKinsey, J.R. Dedman, E.N. Olson, J. Chen, J.H. Brown, and D.M. Bers. 2006. Local InsP3-dependent perinuclear Ca2+ signaling in cardiac myocyte excitation-transcription coupling. *J. Clin. Invest.* 116:675–682. http://dx.doi.org/10.1172/JCI27374

Zhang, X., G. Azhar, S.A. Helms, and J.Y. Wei. 2011. Regulation of cardiac microRNAs by serum response factor. *J. Biomed. Sci.* 18:15. http://dx.doi.org/10.1186/1423-0127-18-15

Zhao, Y., E. Samal, and D. Srivastava. 2005. Serum response factor regulates a muscle-specific microRNA that targets Hand2 during cardiogenesis. *Nature*. 436:214–220. http://dx.doi.org/10.1038/nature03817

Published November 19, 2012

Drawnel et al., http://www.jcb.org/cgi/content/full/jcb.201111095/DC1

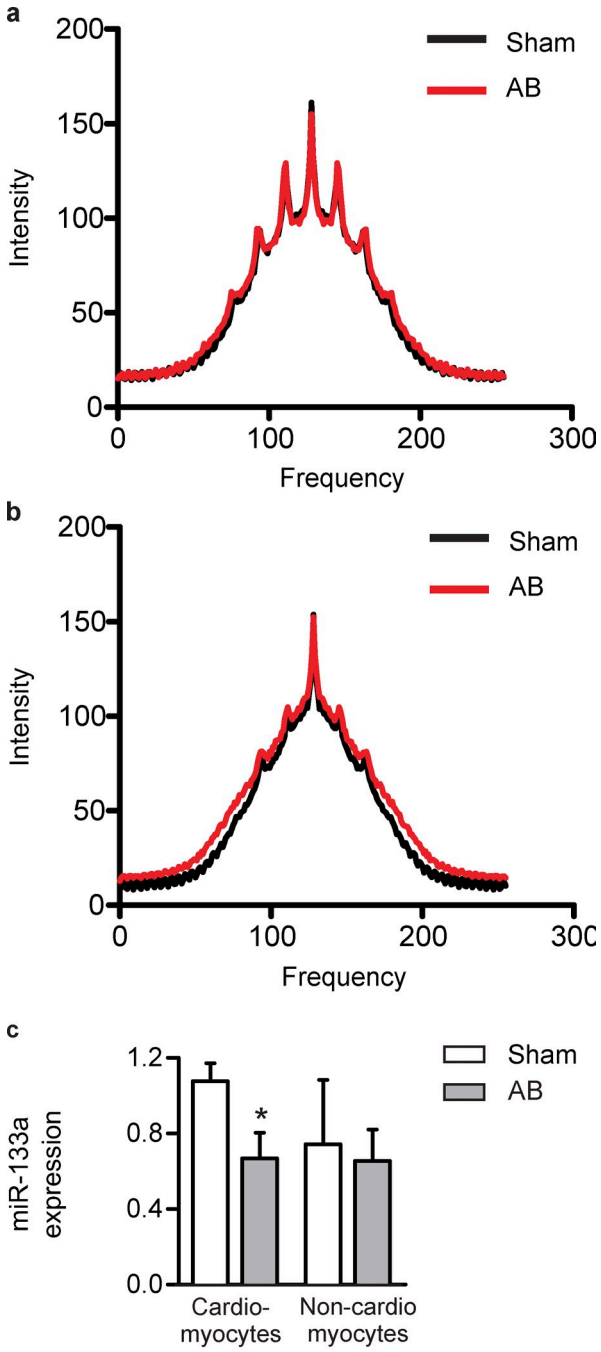

Figure S1. **IP_3RII protein and miR-133a expression is altered in hypertrophic ventricular myocytes.** (a and b) 2D Fourier analysis of deconvolved confocal images of isolated ventricular cardiomyocytes from sham or AB rats immunostained for (a) RyR2 and (b) IP_3RII. Note the increase in the high frequency population of pixels positive for IP_3RII in AB samples and the lack of a corresponding alteration in RyR2 pixel frequency. For the sham condition, 16 cells from 2 independent preparations were analyzed. For the AB condition, 26 cells from 2 independent preparations were analyzed. (c) qPCR quantification of miR-133a expression in sham ($n = 5$) and AB ($n = 4$) cardiomyocyte and sham ($n = 5$) and AB ($n = 5$) noncardiomyocyte cell populations. Data are mean ± SEM. *, $P < 0.05$.

Published November 19, 2012

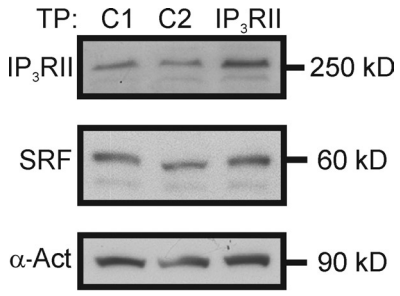

Figure S2. **IP_3RII up-regulation is a specific effect of the IP_3RII target protector.** Immunoblot for IP_3RII in lysates from NRVMs transfected with control target protector oligos C1 and C2 or the miR-133a–specific oligo (IP_3RII). C1 and C2 are designed to target regions of the Itpr2 3′UTR downstream of the miR-133a binding site. α-Actinin is shown as a loading control.

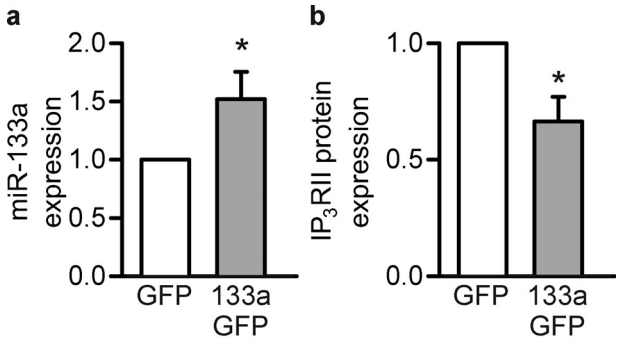

Figure S3. **miR-133a-GFP overexpression down-regulates IP_3RII in ARVMs.** (a) qPCR analysis of miR-133a expression in GFP/miR-133a-GFP overexpressing ARVMs. Data are mean ± SEM from five independent experiments. (b) Quantification of immunoblots for the IP_3RII in GFP/miR-133a-GFP overexpressing ARVMs. Data are mean ± SEM from seven independent experiments. *, $P < 0.05$.

Published November 19, 2012

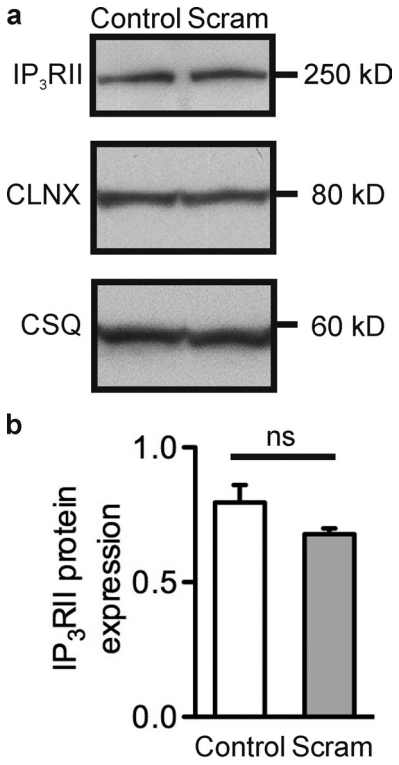

Figure S4. **IP_3RII expression in unaffected by infusion of scrambled miR-133a antagomir.** (a) Immunoblot for IP_3RII in ventricular lysates from control mice or mice infused with a scrambled miR-133a oligonucleotide for 1 mo. CLNX and CSQ are shown as loading controls. (b) Quantification of immunoblots as in panel a. Data are from six control and three scrambled oligonucleotide-treated mice. Bar graphs represent mean ± SEM.

Published November 19, 2012

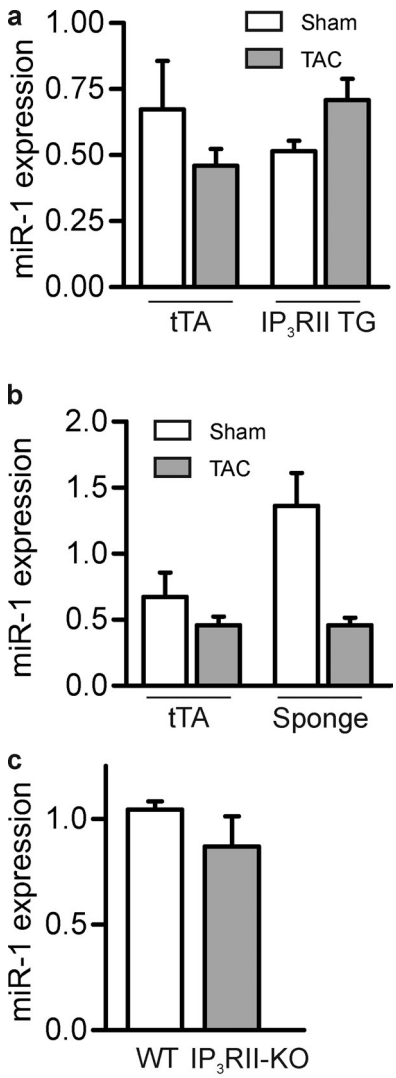

Figure S5. **miR-1 expression is not regulated by IICR.** (a) miR-1 expression measured by qPCR in IP_3RII transgenic mice subjected to sham or TAC procedures. Three mice were analyzed for the tTA sham/TAC and IP_3RII TAC data. Two mice were analyzed for the IP_3RII sham condition. (b) qPCR analysis of miR-1 expression in ventricular lysates from tTA controls and IP_3-sponge (sponge) expressing mice subjected to sham or TAC procedures. Three mice were analyzed for the tTA sham/TAC and sponge-TAC data. Two mice were analyzed for the sponge-sham condition. (c) miR-1 expression measured using qPCR in WT and KO mouse samples. Four WT and four KO mice were analyzed. Data are mean ± SEM.